

The power spectrum  $S$  of linear transects of the earth's topography is often observed to be a power-law function of wave number  $k$  with exponent close to  $-2$ :  $S(k) \propto k^{-2}$ . In addition, river networks are fractal trees that satisfy several power-law relationships between their morphologic components. A model equation for the evolution of the earth's topography by erosional processes which produces fractal topography and fractal river networks is presented and its solutions compared in detail to real topography. The model is the diffusion equation for sediment transport on hillslopes and channels with the diffusivity constant on hillslopes and proportional to the square root of discharge in channels. The dependence of diffusivity on discharge follows from fundamental equations of sediment transport. We study the model in two ways. In the first analysis the diffusivity is parameterized as a function of relief and a Taylor expansion procedure is carried out to obtain a differential equation for the landform elevation which includes the spatially-variable diffusivity to first order in the elevation. The solution to this equation is a self-affine or fractal surface with linear transects that have power spectra  $S(k) \propto k^{-1.8}$ , independent of the age of the topography, consistent with observations of real topography. The hypsometry produced by the model equation is skewed such that lowlands make up a larger fraction of the total area than highlands as observed in real topography. In the second analysis we include river networks explicitly in a numerical simulation by calculating the discharge at every point. We characterize the morphology of real river basins with five independent scaling relations between six morphometric variables. Scaling exponents are calculated for seven river networks from a variety of tectonic environments using high-quality digital elevation models. River networks formed in our model match the observed scaling laws and satisfy Tokunaga side-branching statistics.

## I. INTRODUCTION

A remarkable feature of the earth's surface is its scale-invariance. Objects such as a hammer or a person often need to be included in landscape photographs because features such as variations in height of a topographic profile have no characteristic scale. Similarly, a scale on a map is often necessary to determine whether the map details features at the scale of one kilometer or hundreds of kilometers. The scale-invariance of topography can be quantified with techniques of time series analysis. Variations in the height of a topographic profile can be characterized with the probability density function and the power spectrum. The probability density function quantifies how the data is distributed about the mean. Two examples of probability density functions are the normal and lognormal distributions. The power spectrum  $S$  measures the persistence of the data. The power spectrum is defined as the square of the coefficients in a Fourier series representation of the transect. It measures the average variation of the function at different wavelengths. If adjacent data points are totally uncorrelated then the power spectrum will be constant as a function of wave number (the reciprocal of the wavelength), i.e. white noise. If adjacent values are strongly correlated relative to points far apart the power spectrum will be large at small wave numbers (long wavelengths) and small at large wave numbers (short wavelengths). The power spectrum  $S$  of linear transects of topography have a power-law dependence on wave number with exponent close to  $-2$  over a wide range of scales:  $S(k) \propto k^{-2}$  [Vening Meinesz, 1951; Mandelbrot, 1975; Sayles and Thomas, 1978; Newman and Turcotte, 1990]. Culling and Datko [1987] have obtained equivalent results with the rescaled-range technique. Matsushita and Ouchi [1989] have computed the roughness exponent  $H$  defined by the relationship between the standard deviation and the length  $L$  of the transect,  $\sigma \propto L^H$ , for several topographic transects. They obtained  $H \approx 0.55$  which implies a power spectral exponent of  $\beta = -2.1$  from the relation  $\beta = 2H + 1$  [Turcotte, 1992]. Ahnert [1984] obtained a similar value. Turcotte [1987] and Balmino [1993] have computed the power spectrum from a spherical harmonic representation of the earth's topography and bathymetry. They observed a power spectrum

$S(k) \propto k^{-2}$  at scales less than 10,000 km and an approximately constant spectrum at larger scales. Similar scale-invariance has been identified in the earth's bathymetry [Bell, 1975], the topography of natural rock surfaces [Brown and Scholz, 1985], and the topography of Venus [Kucinskas et al., 1992]. The observation of scale-invariant topography on Venus indicates that fractal topography can be formed without erosion. A power-law power spectrum is indicative of scale-invariance since the power-law function has no length scale in it. Turcotte [1992] has shown that these observations define topography to be a self-affine fractal with a fractal dimension close to 2.5. Synthetic topography which assumes random phases in the Fourier coefficients can be generated which have  $S(k) \propto k^{-2}$  as observed in real topography. Images of synthetic topography with  $S(k) \propto k^{-2}$  produced with techniques described in Voss [1988] and presented in Mandelbrot [1983] resemble natural topography. However, the lack of any river networks in these images indicates that the power spectrum is not a complete representation of the earth's topography [Weissel, Pratson, and Malinverno, 1994]. Gilbert [1989] and Evans and McClean [1995] have documented deviations from scale-invariance of the earth's topography.

Besides the power spectrum, the distribution or hypsometry of topography is an important statistical measure. The topography of the earth's continents are highly skewed such that a much larger percentage of the earth's topography is lowlands (topography with an elevation below the median elevation for a region) and there is a positive correlation between elevation and slope (i.e. as one drives up a mountain, the steepness of the climb increases). This is not predicted by a model with a Gaussian distribution such as the Brownian walk [Weissel, Pratson, and Malinverno, 1994]. This discrepancy between Gaussian models of topography and observed topography is consistent with the observation of Mandelbrot [1983] who found that when he transformed his Gaussian synthetic topography with a cubic function, the topography looked more realistic.

Many studies have attempted to model the evolution of drainage networks. Recent papers have emphasized their fractal properties. Some authors describe discretized models which follow the flow of discrete units of runoff down the steepest slope and erode the hillslope

with an assumed dependence of denudation on slope (and possibly other factors) [Willgoose, Bras, and Rodriguez-Iturbe, 1991; Chase, 1992; Kramer and Marder, 1992; Leheny and Nagel, 1993; Inaoka and Takayasu, 1993; Howard, 1994]. After the drainage of a large number of randomly deposited units of precipitation, a rough landscape is produced. Willgoose *et al.* [1991], Leheny and Nagel [1993], Kramer and Marder [1992], and Inaoka and Takayasu [1993] have shown that their models produce drainage networks consistent with the observed scaling behavior of real drainage networks. Chase [1992] has presented a model that can produce fractal topography with fractal dimensions broadly consistent with observed values. Models have also been proposed which do not explicitly model the landform topography but only the growth of the drainage network. Stark [1991] has proposed a model based on self-avoiding percolation clusters. Kondoh and Matsushita [1986], Meakin, Feder, and Jossang [1991], Masek and Turcotte [1993], and Stark [1994] have presented models based on diffusion-limited-aggregation (DLA) and variants of DLA. In Masek and Turcotte [1993] the random walkers are introduced randomly into the landscape rather than at the boundaries (as in traditional DLA) to better model the effect of storms producing runoff randomly in space and time. Other approaches include that of Newman and Turcotte [1990] who propose a cascade model similar to Kolmogorov's model of the turbulent cascade in which the variance at each scale is dependent only on that scale and the next largest one. Several studies have proposed continuum growth equations. Sornette and Zhang [1993] have advocated a model equation known as the Kardar-Parisi-Zhang (KPZ) equation, originally introduced in the physics literature to model the growth of atomic surfaces by ion deposition [Kardar, Parisi, and Zhang, 1986], as a model for the evolution of topography by geomorphic processes. Newman and Turcotte [1990] and Sornette and Zhang [1993] have stressed the necessity of nonlinear terms in order to produce scale-invariant topography. The KPZ equation is

$$\frac{\partial h}{\partial t} = D\nabla^2 h + \frac{\lambda}{2}(\nabla h)^2 + \eta(x, y, t) \quad (1)$$

where  $\eta(x, y, t)$  is a Gaussian white noise. The first term represents the classic Culling diffusion model of slope erosion. Culling [1960, 1963] hypothesized that the horizontal

flux of eroded material was proportional to the slope. With conservation of mass this yields the diffusion equation. Solutions to the diffusion equation have been successfully applied to modeling the evolution of alluvial fans, incised channels, prograding deltas, and eroding fault scarps [Wallace, 1977; Nash, 1980; Begin *et al.*, 1981; Gill, 1983a,b; Hanks *et al.*, 1984; Hanks and Wallace, 1985; Kenyon and Turcotte, 1985; Phillips and Sutherland, 1986]. McKean *et al.* [1993] have implied diffusion coefficients of hillslope evolution with geochemical methods. They obtained similar diffusion constants to those inferred from modeling fault scarp relaxation. The last term in equation 1 represents spatial variations in erosion intensity produced by the intermittent nature of runoff production and mass movements, spatial variations in the erodibility of the soil and rock of the landscape, and episodic tectonic uplift. The inclusion of a stochastic term such as this is a universal feature of models considered in the physics literature which produce self-affine surfaces. Sornette and Zhang [1993] have argued that the nonlinear term in equation 1 is essential for the formation of a scale-invariant surface. The nonlinear term is equivalent to assuming that the erosion rate is proportional to the local exposed landscape surface. Somfai and Sander [Scaling and river networks: A Landau theory, unpublished manuscript, 1996] have also employed the KPZ equation and have produced landscapes which obey Horton's laws with simulations incorporating only the nonlinear term in the equation for the local erosion rate of the surface. Smith and Bretherton [1972] have presented a generalized model of hillslope evolution which includes the KPZ nonlinear term as a special case. Giacometti, Maritan, and Banavar [1995] have proposed a continuum growth equation that includes higher order terms not present in the KPZ equation.

It should be emphasized that a great variety of models, including most of those listed, obey Horton's laws. Horton's laws state that stream number, average stream length, and average drainage area decrease geometrically with stream order defined by the Strahler ordering scheme. Since so many different models obey Horton's laws, agreement with Horton's laws does not appear to be sufficient to verify that a model is an accurate representation of drainage network formation [Willgoose, 1994]. In fact, Kirchner [1993] has argued that

Horton’s laws are satisfied by virtually all possible branching networks. *Tokunaga* [1984] and *Peckham’s* [1995] improved classification of stream order appears to be a more stringent test for models and is a significant advance in this regard.

In this paper we investigate a model of landform evolution with topographic evolution by geomorphic processes parameterized with the diffusion equation. The model we propose reproduces the observed statistical behavior of both topography and river networks. The diffusion equation models the relaxation of topographic variations by overland and channel flow. In Section 2 we present a derivation due to *Begin, Meyer, and Schumm* [1981] which shows diffusivity to be proportional to the square root of the discharge. It is this dependence on discharge, itself dependent on the basin morphology, that gives rise to a complex unstable behavior from such a simple model. Our first analysis of the model will be to parameterize the diffusivity as a function of relief and perform a Taylor expansion retaining the spatial variability of diffusivity to first order in the elevation. A nonlinear partial differential equation is derived and solved which reproduces the hypsometry and power-spectral behavior of real topography. In Section 4 numerical simulations are performed which explicitly include river networks and calculate the discharge at every point. Realistic river networks and topography are generated.

## II. DEPENDENCE OF DIFFUSIVITY ON DISCHARGE

*Begin, Meyer, and Schumm* [1981] have derived the diffusion equation for channel evolution using similar assumptions to those used by *Culling* [1960, 1963] for hillslope evolution. Their derivation began with classic equations of sediment transport. They showed diffusivity to be proportional to the discharge per unit width above a point on the surface. The authors began with a commonly observed empirical relationship between sediment flux  $Q_s$  and bottom shear stress  $\tau$ :

$$Q_s \propto \tau^{\frac{3}{2}} \quad (2)$$

The mean flow velocity above a point on the surface is

$$v = \left( \frac{8}{f} g R \frac{\partial h}{\partial x} \right)^{\frac{1}{2}} \quad (3)$$

where  $f$  is the Darcy-Weisbach factor,  $g$  is the acceleration due to gravity,  $R$  is the hydraulic radius, and  $\frac{\partial h}{\partial x}$  is the channel slope along the length of the longitudinal profile of a channel. For wide channels,  $v = Q_w/R$  where  $Q_w$  is the water discharge per unit width. Substituting this relation into equation 3, *Begin, Meyer, and Schumm* [1981] obtained

$$R = Q_w^2 \left( \frac{f}{8g \frac{\partial h}{\partial x}} \right)^{\frac{1}{3}} \quad (4)$$

Substituting the expression for  $R$  into the equation  $\tau = \rho g R \frac{\partial h}{\partial x}$ , where  $\rho$  is the density of water, gives

$$\tau \propto \left( \frac{\partial h}{\partial x} \right)^{\frac{2}{3}} \quad (5)$$

Substituting this into equation 2 results in the following expression for sediment discharge

$$Q_s \propto Q_w \frac{\partial h}{\partial x} \quad (6)$$

Since  $\frac{\partial h}{\partial t} = \frac{\partial Q_s}{\partial x}$  by conservation of mass, equation 6 gives a diffusion equation for the channel elevation with a diffusivity propotional to the water discharge per unit width:

$$\frac{\partial h}{\partial t} = c Q_w \frac{\partial^2 h}{\partial x^2} \quad (7)$$

where  $c$  is a constant dependent on  $f$ ,  $g$ , and  $\rho$ . The diffusion model and a discharge-dependent diffusivity is consistent with the laboratory measurements of aggradation and degradation in channels by *Gill* [1983a,b] and *Phillips and Sutherland* [1986].

Since the width of a river is proportional to the square root of the discharge [*Leopold, Wolman, and Miller*, 1964], the diffusivity of a channel is proportional to  $Q/w \propto Q/Q^{\frac{1}{2}} \propto Q^{\frac{1}{2}}$ , the square root of the discharge. In our model we will have a constant diffusivity on hillslopes and a diffusivity proportional to the square root of discharge in channels:

$$\begin{aligned} \frac{\partial h}{\partial t} &= \nabla(D(Q)\nabla h) \\ D &= \text{if the site is a hillslope} \\ D &\propto Q^{\frac{1}{2}} \quad \text{if the site is a channel} \end{aligned} \quad (8)$$

In order to solve this equation it is necessary to parameterize discharge in terms of the morphology of the basin. Discharge is principally a function of drainage basin area. It is often assumed that discharge and area are proportional [*Rodriguez-Iturbe et al.*, 1992]. However, in an analysis of 350 of the world's largest river basins, *Mulder and Syvitski* [1996] have established the relationship between average discharge and drainage area to be a power-law relationship with exponent 0.75:  $Q_{av} \propto A^{0.75}$ . This means that larger basins drain less water per unit area than small basins. One interpretation of this observation is that more infiltration occurs in large basins. To test this hypothesis, *Mulder and Syvitski* [1996] related the average discharge  $Q_{av}$  to the basin area corrected by the cosine of the average basin slope,  $A/\cos\alpha$ . They obtained a correlation coefficient of 0.9 with this expression compared to 0.74 for the power-law relationship, lending support to the hypothesis. However, in order to maintain consistency with the power-law relationships we will identify between the morphometric variables, we will relate discharge to drainage area using the power-law relationship  $Q_{av} \propto A^{\frac{3}{4}}$ . The model equation as a function of area is then

$$\begin{aligned} \frac{\partial h}{\partial t} &= \nabla(D(A)\nabla h) \\ D &= D_h \text{ if the site is a hillslope} \\ D &\propto (Q^{\frac{1}{2}})^{\frac{3}{4}} = D_c A^{\frac{3}{8}} \text{ if the site is a channel} \end{aligned} \tag{9}$$

### III. APPROXIMATE SOLUTION OF THE MODEL EQUATION

Discharge is a function of basin relief, the difference in elevation between the highest and lowest points in the basin. In first-order streams high in mountainous areas the discharge is very small compared to that for lowland rivers. In this section we parameterize the discharge as a function of relief to obtain a single differential equation for the local elevation in space and time,  $h(x, y, t)$ . The equation is solved and its solutions are found to have a hypsometry and power spectrum comparable to those of real topography dominated by erosional processes.



In Section 4 we will present the results of morphometric analyses of river networks. We will show the drainage area to be a power function with exponents between 3 and 5 of the basin relief,  $h - h_{max}$ , where  $h$  is the elevation of the outlet and  $h_{max}$  is the maximum elevation of the basin. Since the diffusivity is defined to be a power-law function of drainage area, the dependence of the diffusivity on relief is also a power law with exponent  $a$ :

$$D \propto (h - h_{max})^a \quad (10)$$

$D$  can be expanded in a Taylor series for small  $h$ :  $D \approx D_0 - D_1 h$  where  $D_0$  and  $D_1$  are positive constants.

The diffusion equation with spatially variable diffusivity is

$$\begin{aligned} \frac{\partial h}{\partial t} &= \nabla(D(h/h_{max})\nabla h) \\ &= D(h/h_{max})\nabla^2 h + \frac{\partial D}{\partial h}(\nabla h)^2 \end{aligned} \quad (11)$$

The diffusivity must be kept inside the gradient term since it is not a constant. The chain rule has been used.

Substituting equation 10 into equation 11 and keeping only terms first order in  $h$  gives

$$\frac{\partial h}{\partial t} = D_0 \nabla^2 h - D_1 (\nabla h)^2 \quad (12)$$

The effects of the terms in equation 12 are illustrated in Figures 1 and 2. In Figure 1a, the topography at time  $t$  is assumed to be given by a Gaussian function. The topography is taken to be one-dimensional for the purposes of illustration. The rate of change of the surface resulting from the diffusion term is given in Figure 1b and the surface at time  $t + \Delta t$  is shown in Figure 1c. The effect of the diffusion term is to aggrade the topography where the surface is concave up and erode where the surface is concave down. The topography of the surface at time  $t + \Delta t$  is also a Gaussian function.

In contrast, the nonlinear term does not preserve the Gaussianity of the initial surface. Figure 2 presents the same sequence of graphs for the nonlinear term. The term erodes

material where the slope is large resulting in a more concave topography with a skewed hypsometry and a larger fraction of topography in lowlands compared to the original Gaussian function.

Equation 12 is completely deterministic. However, there is abundant empirical evidence that spatially and temporally variable erosion rates are universal over a wide range of time and length scales. Much of the sediment carried away in rivers is carried away in intermittent storms whose occurrence can only be described statistically. An example of this intermittency is the time series of sediment load in the Santa Clara River. The sediment load of the Santa Clara was carefully monitored for a period of 18 years. Over half of the total sediment yield carried by the river was transported in only three large floods totaling seven days [Milliman and Syvitski, 1992]. Similar large bursts of sediment transport are evident in the sediment transport time series of Plotnick and Prestegard [1993] on time scales of hours. Many examples of large floods which have resulted in major landscape modification have been documented in the geologic record [Bretz, 1969; Meyer and Nash, 1983; Ager 1993]. Spatially and temporally variable erosion rates have been documented over a variety of spatial and temporal scales and geomorphological settings [Luk, 1982; Ormi, 1982; Schmidt, 1985]. A steady-state competition between intermittent stochastic forcing and subsequent relaxation of the landscape has been argued to be the essential dynamic of landscape evolution [Wolman and Gerson, 1978]. A model of landscape evolution as a sequence of episodic events is consistent with the age distributions of rock avalanches and sedimentary sequences [Griffiths, 1993]. These observations suggest that any model of landform evolution must include stochastic spatial and temporal variability in erosion rates. If we include spatial and temporal variations in erosion rates by adding a Gaussian white noise erosion rate,  $\eta(x, y, t)$ , to equation 12, the result is the KPZ equation (equation 1).

The solution to the KPZ equation is a self-affine or fractal surface with linear transects that have power-law power spectra with an exponent of  $-1.8$ :  $S(k) \propto k^{-1.8}$  [Amar and Family, 1989]. This is concluded by relating the Hausdorff measure reported for the KPZ model,  $H \approx 0.4$ , to the one-dimensional power spectral exponent,  $\beta$ , through the relation

$\beta = 2H + 1$  [Turcotte, 1992]. Due to the difficulty of solving nonlinear partial differential equations numerically [Newman and Bray, Strong-coupling behavior in discrete Kardar-Parisi-Zhang equations, unpublished manuscript, 1996], a cellular automaton model, the restricted solid-on-solid (RSOS) model, has been developed by Kim and Kosterlitz [1989] with rules that mimic the terms in the KPZ equation. Park and Kahng [1995] have shown that the RSOS model is equivalent to the KPZ equation in the continuum limit. In the RSOS model, a site on a two-dimensional lattice of points is chosen at random. The height of the surface at that point is incremented by one if the elevation at that point is greater than or equal to the elevations of all of its four nearest neighbors. If this restriction is not satisfied, nothing happens. This rule is repeated until a surface with a height equal to or greater than the linear dimension of the lattice is generated. Periodic boundary conditions are used. We performed simulations of this model on a 256 x 256 lattice. A shaded relief image of an example of a surface generated with this model is shown in Figure 3. The average power spectrum, estimated as the square of the coefficients of the Fast Fourier Transform, of linear transects of this surface is presented in Figure 4. The power spectrum of each row of the lattice was computed and then averaged with the power spectra of all other rows in order to obtain the average power spectrum. A good match with the power spectrum  $S(k) \propto k^{-1.8}$ , indicated by the straight line, is obtained. This power spectrum agrees with the finite difference calculation of the KPZ equation of Amar and Family [1989]. This power spectrum is close to the spectrum  $S(k) \propto k^{-2}$  observed in erosional topography by Huang and Turcotte [1989] and others. The power spectral behavior observed in real topography is independent of the age of the topography (time since significant uplift occurred) and the initial relief following tectonic uplift. For instance, young, rough mountain ranges, such as the Rocky Mountains, exhibit the same power spectral exponent or fractal dimension as smooth mountain ranges such as the Appalachians. Similarly, in the RSOS model a steady-state condition is achieved once a rough surface is produced. In the steady-state condition, the smoothing effects of the diffusion term are balanced by the roughening effects and the power spectral behavior is independent of time. A rougher landscape, defined as a larger

variance per unit wavelength, can be produced by increasing the ratio of the variance of the stochastic term to the diffusion constant. Rougher topography has a larger power spectral density. However, the power spectral exponent, which quantifies the relative amplitude of topography at different wavelengths, is the same for rough or smooth topography.

The topography of the earth’s surface is skewed such that a much larger percentage of the earth’s topography is lowlands and there is a positive correlation between elevation and slope. This skew can be associated with the nonlinear term in equation 11. If only the diffusion term were present, the resulting topography would have a Gaussian distribution. This is because any linear transformation of a function with a Gaussian distribution, such as the noise term in equation 1, results in a function with a Gaussian distribution. The probability density function (p.d.f.) of elevations (hypsometry) produced by the RSOS model is presented in Figure 5a. The p.d.f. was computed using the surfaces generated from 10 simulation runs. The observed p.d.f. is not Gaussian, but is skewed slightly such that the most probable elevation is below the mean elevation of the landscape, i.e. more of the total landscape area is represented by lowlands than highlands. The skew of the distribution increases as the ratio  $D_1/D_0$  increases. The probability distributions for the Kentucky and Mississippi River basins are given in Figures 5b and 5c, respectively. The ETOPO5 dataset [Loughridge, 1986] was used to compute the hypsometry of the Mississippi River basin and the USGS 1deg DEMs [United States Geological Survey, 1990] were used to compute the hypsometry of the Kentucky River basin. Both hypsometries exhibit skew towards lower elevations. This skew is directly comparable to the skew in the RSOS topography and can be associated with the nonlinear term.

Figure 6a-c shows the cumulative percentage of area larger than a given area computed by Harrison *et al.* [1983] using the ETOPO5 dataset [Loughridge, 1986] for the continents of Africa, North America, and South America, with a least-square fit to a lognormal distribution. The hypsometric curves presented in the independent study of Cogley [1985] are similar to those presented in Harrison *et al.* [1983]. The calculated hypsometric curves appear to approach a skewed lognormal distribution as the age since significant uplift increases. Of

the three continents, Africa has experienced the least neotectonic uplift. South America has experienced the most. The hypsometry of Africa matches a lognormal distribution more closely than South America where the presence of the relatively young Andes mountains results in a significant deviation from a lognormal distribution. This suggests that continental hypsometric curves approach a lognormal distribution as erosion has more time to act on the landscape.

#### IV. RIVER NETWORKS

The objective of this section is to incorporate river networks into equation 9. There are several power-law relationships between the morphologic components of river basins. Some of these components are based on the Strahler ordering scheme. In this scheme, a stream with a channel head is defined as a first-order stream. When two like-order streams combine they form a downstream segment one order higher than the order of the tributary streams. A partial list of the observed morphological relations in natural river networks is:

1) *Horton* [1945] defined three ratios,  $R_B$ ,  $R_L$ , and  $R_A$  to be the ratio between the number, average length, and average drainage area from the streams of one order to those of the next lowest order. He found this ratio to be a constant for all stream orders. The fractal dimension of river networks is defined as  $D = \log R_B / \log R_L$ .  $D$  is usually found to be approximately 1.9 [*Turcotte*, 1992].

2) An improved classification scheme leading to a relation similar to Horton's laws has been developed by *Tokunaga* [1984] and *Peckham* [1995]. They defined matrix elements  $T_{o,k}$  as the number of side tributaries of order  $k$  of streams of order  $o$ . Natural river networks satisfy the constraint that  $T_{o,o-k}$  is constant for all  $o$ . Shreve's classic random topology model [*Shreve*, 1966] fails to satisfy this constraint [*Peckham*, 1995]. The classic DLA growth model satisfies this property [*Ossadnik*, 1992].

3) *Hack* [1957] found that the length of a main channel length scales with the drainage area according to power law:  $L \propto A^q$ . He reported values of  $q \approx 0.6$  for two river basins.

*Gray* [1961] obtained a value of 0.57. Some other morphometric analyses based on hundreds of river basins, however, have found no significant deviation from 0.5 [*Montgomery and Dietrich*, 1992; *Mulder and Syvitski*, 1996].

4) Along-channel slope is a power law function of discharge with exponent close to  $-1/2$ :  $S \propto Q_{av}^{-\frac{1}{2}}$  [*Carlston*, 1968]. If it is assumed that discharge and area are proportional, this implies that channel slope is inversely proportional to the square root of the drainage area:  $S \propto A^{-\frac{1}{2}}$ . This assumption is often made and the relationship  $S \propto A^{-\frac{1}{2}}$  is considered to be a universal feature of river networks [*Tarboton et al.*, 1989]. However, as we have pointed out, average discharge and drainage area are not proportional. Thus, one of the two relationships  $S \propto Q_{av}^{-\frac{1}{2}}$  or  $S \propto A^{-\frac{1}{2}}$  should be considered suspect.

The fractal properties of river networks have been reviewed by many authors including *LaBarbera and Rosso* [1989], *Beer and Borgas* [1993], *Nikora* [1994], and *Maritan et al.* [1996]. *Abrahams* [1984] has reviewed other empirical relations observed for river basin morphology such as the statistics of junction angles.

In order to better characterize the morphometric relations between drainage basin components we have carried out river network extraction and analyses on seven basins from a variety of tectonic environments using high-quality Digital Elevation Models. Four river networks were chosen from the composite DEM of *Fielding et al.* [1994]. This data set has 80 m resolution and does not rely on the interpolation of contour lines. Such interpolation, as is done in the USGS 1deg DEMs, may lead to biased slope estimates. Three of these basins are located along the Himalayan front in Nepal, Kumaun, and Bhutan. The fourth is located in the Shanxi Province, China and is formed in loess. This basin has an unusually ordered shape characterized by a high degree of symmetry and unusually straight valleys. The remaining three networks are located in North America. The Kentucky River basin and Schoharie Creek basin were extracted from USGS 1deg DEMs [*United States Geological Survey*, 1990]. The Mississippi River basin was chosen so that a large basin was represented. The Mississippi was extracted from the ETOPO5 data set [*Loughridge*, 1986]. The seven basins are plotted in Figure 7. Although the river network extraction and analyses were

carried out down to the pixel size of the DEM, only rivers with Strahler orders larger than three were plotted so that the network can be identified. The river network extraction and analyses were carried out with RiverTools 1.01 [Peckham, 1997].

The analyses we carried out enable us to identify five independent morphologic relationships between six components. The results are shown in Figures 8 through 12 and are summarized in Table 1. The six morphometric components are stream number of a particular Strahler order  $N$ , Strahler order  $o$ , main channel length  $L$ , drainage area  $A$ , basin relief  $R$ , and along-channel slope  $S$ . The relationships between the variables are defined as

$$N \propto A^p \quad (13)$$

$$L \propto A^q \quad (14)$$

$$S \propto A^r \quad (15)$$

$$R \propto A^s \quad (16)$$

$$A \propto t^o \quad (17)$$

Figure 8 presents the total number of streams of a given Strahler order as a function of the average basin area for that Strahler order for each of the seven basins. The order of plots in Figures 8-13 is, from top to bottom, the Kumaun basin, the Loess plateau of the Shanxi Province, Schoharie Creek, the Nepal basin, the Kentucky River basin, the Mississippi River basin, and the Bhutan river basin. The plots are offset so that they may be placed on the same graph. Figure 8 indicates that  $N$  is approximately proportional to  $A^{-1}$  indicating that  $p \approx -1$ .

Figure 9 presents the relationship between  $L$  and  $A$ . The plots indicate that  $q \approx 0.5$ . There has been considerable debate about whether  $q$  approaches 0.5 exactly or whether there is a significant deviation. The reason for the debate is that if  $q \neq 1/2$  then this may represent a deviation from self-similarity [Ijjasz-Vasquez *et al.*, 1993]. Our analyses exhibit a variation in  $q$  from basin to basin that is roughly equal to the previously reported deviations from  $1/2$ . Therefore, we cannot definitively conclude whether  $q$  differs from  $1/2$  in river basins as a general rule.

Figure 10 indicates that  $r \approx 3/8$ . This is inconsistent with previous studies that have reported  $S \propto A^{-\frac{1}{2}}$  [Tarboton *et al.*, 1989]. The value  $r \approx 3/8$  is entirely consistent with the observed relationships of channel slope to discharge and the scaling of discharge and drainage area:  $S \propto Q_{av}^{-\frac{1}{2}}$  and  $Q_{av} \propto A^{\frac{3}{4}}$  implies  $S \propto A^{\frac{3}{8}}$ , as observed. The work of Tarboton *et al.* [1989] carried out analyses on two river basins with three orders-of-magnitude of area in the analyses. Given that our analyses were carried out on several basins with five orders-of-magnitude of area with a high-quality DEM we propose that  $r \approx 3/8$  is a more reliable estimate. This conclusion appears to be consistent with the data of Montgomery and Dietrich [1988] who presented similar slope-area relationships. Although no exponents were obtained, the trends of their data follow a power-law relationship with exponent significantly greater than  $-1/2$  (i.e. closer to  $-3/8$ ).

The observed scaling between along-channel slope and drainage area follows directly from equation 9. The flux of sediment is given by  $Q_s = D_c A^{\frac{3}{8}} \frac{\partial h}{\partial x}$ . For a longitudinal profile in equilibrium,  $\frac{\partial Q_s}{\partial x} = 0$ .  $\frac{\partial Q_s}{\partial x} = 0$  implies that the average slope  $\frac{\partial h}{\partial x}$  must be related to drainage area  $A$  as  $\frac{\partial h}{\partial x} \propto A^{-\frac{3}{8}}$  as observed.

Plotted in Figure 11 are the relationships between relief  $R$  and area  $A$ . A range of values is observed between  $s \approx 1/5$  and  $s \approx 1/3$ .

The relationship between basin area and Strahler order  $o$  is plotted in Figure 12. In this figure area is plotted on a logarithmic (base 10) scale while Strahler order is plotted on a linear scale. The slopes are observed to be approximately  $2/3$ . Thus, the Horton ratio  $R_A$  is equal to  $10^{\frac{2}{3}} \approx 4.6$ . Using the other morphometric relations, we can estimate  $R_L$  and  $R_B$  as 2.2 and 4.6, respectively.

The results of Tokunaga side-branching statistical analyses on the seven drainage basins is presented in Figure 13. In this ordering scheme matrix elements  $T_{o,k}$  are defined to be the number of side tributaries of Strahler order  $k$  of streams of Strahler order  $o$ . Natural river networks satisfy the constraint that  $T_{o,o-k}$  is constant for all  $o$ . We have determined  $T_k$  by averaging the vales of  $T_{o,o-k}$  over  $o$ :



$$T_k = \frac{1}{n-k} \sum_{o=1}^{n-k} T_{o,o-k} \quad (18)$$

Plotted in Figure 13 is  $T_k$  on a logarithmic (base 10) scale as a function of  $k$  on a linear scale. The plots indicate that  $T_k \propto u^k$  where  $u$  is estimated to be  $10^{0.4} \approx 2.5$ .

We now consider the numerical simulation of equation 9. The resulting model river networks will be analyzed in the same manner as the real river networks analyzed above. The equation was simulated on a square lattice of 64 x 64 grid points. The equation was discretized in space and time. Integration in time utilized the predictor-corrector method which varies the time step to ensure stability. The initial condition was an elevation of 1.0 on every point of lattice except for the upper left corner which was moved down to 0.0 at  $t=0$  and fixed to be zero for the entire calculation. The slope at all of the edges was fixed to be 0.1 except for the upper left corner which was unconstrained. This constraint on slope at the boundaries is necessary because either the elevation or its derivative must be specified at the boundaries. Since the largest slopes in a basin are in mountainous streams far from the basin outlet, imposing a significant slope on the boundary gridpoints while allowing the elevations to be unconstrained as the drainage divide advances or retreats appeared to be the most realistic boundary condition. The contributing area at each point was continuously updated. Each grid point drained to the lowest of its nearest neighbors. If a grid point was moved up or down such that it no longer was the lowest neighboring grid point for one of its neighbors, the contributing area of each grid point downhill of the old drainage path was decremented by one and the contributing area of each grid point downhill of the new drainage path was incremented by one.

Since we are modeling the hillslope and the river network as distinct states, we must model the growth of the channels into the hillslope. It may be of interest to model fluctuations in the topography with a river network already formed, but a complete model of landscape evolution must consider the feedback between a growing network and the topography of the adjacent hillslopes. One simple way to model growth of the network is to start a simulation with one or more small channels draining to the border of the lattice and

extend the channel from these locations at a given rate when the area drained by the grid point, a proxy for discharge, exceeds a given threshold. Such a model of headward growth is supported by field studies [*Patton and Schumm, 1975; Begin and Schumm, 1979*]. It was also used in the model of *Willgoose, Bras, and Rodriguez-Iturbe [1991]*. In our model the threshold for channelization was set to be zero so that every point in the lattice eventually became a channel. The rate of channel advancement is governed by conservation of mass. For the channel to advance a distance  $\Delta x$ , the mass that must be moved downstream is equal to  $\frac{\partial h}{\partial x} \Delta x$  where  $\frac{\partial h}{\partial x}$  is the slope along the longitudinal profile. Since the flux is equal to  $D(A) \frac{\partial h}{\partial x}$ , the rate of channel advancement is proportional to  $D(A)$ .

Greyscale plots of the elevations of the model surface for four instants of time are plotted in Figure 14a-d. The surface elevations are mapped to a brightness scale with a gamma function with a coefficient of 2.0. The four instants of time correspond to those where (a) 1/8 , (b) 1/4, (c) 1/2, and (d) all of the lattice has become channelized. Despite the fact that the simulation is fully deterministic and begins with symmetric boundary conditions, an asymmetric basin morphology is produced as a result of the instability of channel downcutting. As a river basin cuts down its valley, the river basin increases its drainage area. This further enhances channel downcutting and so on. Thus, any difference in basin drainage area tends to be amplified over time by this instability.

In Figure 15a, the river network corresponding to the surface of Figure 14d is presented. In this plot the river width is made equal to the Strahler order so that thicker rivers indicate those that drain more area. In Figure 15b is plotted the river network created with the same parameters as Figure 15a but with some stochastic variability included in the sediment transport. For each pixel and each time step, a factor  $(1 + 0.1\eta)$  was multiplied times  $\Delta h$ , where  $\eta$  is a Gaussian white noise with mean zero and standard deviation of one. As previously argued, spatial and temporal variations in erodibility are a universal feature of landscape evolution. The purpose of including this stochastic variability was to determine its effect, if any, on the morphology of the basin.

Figures 16-21 are plots of the morphologic relationships corresponding to those for real

river basins presented in Figure 8-13. In these plots three river basins are analyzed. The results for the deterministic simulation of resulting in the basin of Figure 14d are presented as the top graph. The middle graph represents the results of morphometric analyses on the partially-developed river basin of Figure 14c. The results of the stochastic river basin illustrated in Figure 15b are presented as the bottom graph. The results of the morphometric analyses on the real and model river basins are summarized in Table 1.

The same scaling relations are observed for the three model river basins, suggesting that the scaling laws we have identified are satisfied by river basins continuously as they evolve by headward growth and that they are satisfied even in the presence of heterogeneous erodibility and/or runoff. Close agreement between model and real river basins was observed for most of the morphometric relationships. The scaling exponent of slope  $S$  and area  $A$  was observed to be slightly higher for the model river networks (-0.29 to -0.32) compared to the observed value of approximately  $-0.37$  in real river basins. This was unexpected since the result  $S \propto A^{-0.37}$  is satisfied exactly for a river basin in equilibrium (where the sediment flux is everywhere constant). The reason for this discrepancy will require further study. In addition, the Horton ratio  $R_A$  and the Tokunaga exponent  $u$  quantified in Figures 20 and 21 were about 20% higher for the model basins than for the real river basins. Nevertheless, the broad consistency between the observed relations and those satisfied by the model suggests that this model captures the essential dynamics of self-organization in river basins.

The probability density function of the model basin of Figure 15a is presented in Figure 22. As observed in the Kentucky and Mississippi River basins, the hypsometry is skewed such that the most probable elevation is lower than the median elevation. The evolution of the hypsometric curve (cumulative distribution function) for the model basins of Figure 14a-d is shown in Figure 23 as the top to bottom graphs, respectively. A close similarity exists between this sequence and the evolution observed in real basins. As an example, in Figure 24 we show the hypsometric curves observed over time at Perth Amboy, New Jersey by *Schumm* [1956]. Both the real and model basins begin with a nearly constant surface equal to the maximum elevation of the basin. As the channels dissect the basin, the hypsometric

curve smooths out. The basins reach equilibrium with a skewed p.d.f. as evidenced by the fact that the model and real hypsometric curves fall below  $1/2$  at a normalized elevation of  $1/2$ . A Gaussian or any other symmetric distribution would pass through  $(1/2, 1/2)$ .

## V. CONCLUSIONS

We have presented a model of landscape evolution by overland and channel flow which reproduces many of the basic statistical features of topography and river basin morphology. The model is based on the observation that channel and hillslope adjustment by sediment transport can often be modeled by the diffusion equation with a diffusivity dependent on discharge. The dependence of diffusivity on discharge introduces a nonlinear term in the partial differential equation for landscape elevation which is responsible for the fractal nature of topographic transects and results in a characteristic hypsometric curve. The morphometric relationships for seven river basins have been computed and have been found to be remarkably universal. Model drainage basins have morphologies which closely approximate those observed in nature.

## VI. ACKNOWLEDGEMENTS

I wish to thank Chris Duncan and Don Turcotte for helpful conversations. Special thanks is extended to Scott Peckham for making RiverTools 1.01, his remarkable river network and extraction program, available over the Internet. Most of this work would not have been possible without Scott's program. This work was supported in part by NASA grant NAGW-4702.

---

[1] Ager, D.V., *The New Catastrophism*, Cambridge Univ. Press, New York, 1993.

- [2] Ahnert, F., Local relief and the height limits of mountain ranges, *Am. J. Sci.*, *284*, 1035-1055, 1984.
- [3] Amar, J.G., and F. Family, Numerical solution of a continuum equation for interface growth in 2+1 dimensions, *Phys. Rev. A*, *41*, 3399-3402, 1989.
- [4] Balmino, G., The spectra of the topography of the earth, Venus, and Mars, *Geophys. Res. Lett.*, *20*, 1063-1066, 1993.
- [5] Barabasi, A.-L., and H.E. Stanley, *Fractal Concepts in Surface Growth*, Cambridge Univ. Press, New York.
- [6] Beer, T., and M. Borgas, Horton's laws and the fractal nature of streams, *Water Resour. Res.*, *29*, 1475-1487, 1993.
- [7] Begin, Z.B., Application of "diffusion" degradation to some aspects of drainage net development, in *Badland Geomorphology and Piping*, edited by R. Bryan and A. Yain, pp. 169-179, Geobooks, Norwich, 1982.
- [8] Begin, Z.B., and S.A. Schumm, Instability of alluvial valley floors: A method for its assessment, *Trans. ASAE*, *22*, 347-350, 1979.
- [9] Begin, Z.B., D.F. Meyer, and S.A. Schumm, Development of longitudinal profiles of alluvial channels in response to base level lowering, *Earth Surf. Processes*, *6*, 49-68, 1981.
- [10] Bell, T.H., Statistical features of sea-floor topography, *Deep-Sea Res.*, *22*, 883-892, 1975.
- [11] Bretz, J.H., The Lake Missoula floods and the channeled scablands, *J. Geol.*, *77*, 505-543, 1969.
- [12] Brown, S.R., and C.H. Scholz, Broad bandwidth study of the topography of natural rock surfaces, *J. Geophys. Res.*, *90*, 12575-12582, 1985.
- [13] Carlston, C.W., Slope-discharge relations for eight rivers in the United States, *U.S. Geol. Surv. Prof. Pap.*, *600*, 45-47, 1968.

- [14] Chase, C.G., Fluvial land sculpting and the fractal dimension of topography, *Geomorphology*, 5, 39-57, 1992.
- [15] Cogley, J.G., Hypsometry of the continents, *Z. Geomorph. N. F. Supp.*, 53, 1-48, 1985.
- [16] Culling, W.E.H., Analytical theory of erosion, *J. Geol.*, 68, 336-344, 1960.
- [17] Culling, W.E.H., Soil creep and the development of hillside slopes, *J. Geol.*, 71, 127-161, 1963.
- [18] Culling, W.E.H., and M. Datko, The fractal geometry of the soil-covered landscape, *Earth Plan. Sci. Lett.*, 12, 369, 1987.
- [19] Evans, I.S., and C.J. McClean, The land surface is not unifractal: variograms, cirque scale, and allometry, *Z. Geomorph. N. F. Supp.*, 101, 127-147, 1995.
- [20] Fielding, E., B. Isacks, M. Barazangi, and C.C. Duncan, How Flat is Tibet?, *Geology*, 22, 163-167, 1994.
- [21] Giacometti, A., A. Maritan, and J.R. Banavar, Continuum model for river networks, *Phys. Rev. Lett.*, 75, 577-580, 1995.
- [22] Gilbert, L.E., Are topographic datasets fractal?, *Pure and Appl. Geophys.*, 131, 241-254, 1989.
- [23] Gill, M.A., Diffusion model for aggrading channels, *J. Hyd. Res.*, 21, 355-367, 1983.
- [24] Gill, M.A., Diffusion model for degrading channels, *J. Hyd. Res.*, 21, 369-378, 1983.
- [25] Griffiths, G.A., Estimation of landform life expectancy, *Geology*, 21, 403-406, 1993.
- [26] Gray, D.M., Interrelationships of watershed characteristics, *J. Geophys. Res.*, 66, 1215-1223, 1961.
- [27] Hack, J.T., Studies of longitudinal profiles in Virginia and Maryland, *U.S. Geol. Surv. Prof. Pap.*, 294B, 1957.
- [28] Hanks, T.C., R.C. Buckman, K.R. Lajoie, and R.E. Wallace, Modification of wave cut and faulting-controlled landforms, *J. Geophys. Res.*, 89, 5771-5790, 1984.

- [29] Hanks, T.C., and R.E. Wallace, Morphological analysis of the Lake Lahontan shoreline and beachfront fault scarps, Pushing County, Nevada, *Bull. Seismol. Soc. Am.*, *75*, 835-846, 1985.
- [30] Harrison, C.G.A., K.J. Miskell, G.W. Brass, E.S. Saltzmann, and J.L. Sloan II, Continental hypsometry, *Tectonics*, *2*, 357-378, 1983.
- [31] Horton, R.E., Erosional development of streams and their drainage basins: Hydrophysical approach to quantitative morphology, *Bull. Geol. Soc. Am.*, *56*, 275-370, 1945.
- [32] Howard, A.D., A detachment-limited model of drainage basin evolution, *Water Resour. Res.*, *30*, 2261-2285, 1994.
- [33] Huang, J., and D.L. Turcotte, Fractal mapping of digitized images: Applications to the topography of Arizona and comparisons with synthetic images, *J. Geophys. Res.*, *94*, 7491-7495, 1989.
- [34] Ijjasz-Vasquez, E.J., R.L. Bras, and I. Rodriguez-Iturbe, Hack's relation and optimal channel networks: the elongation of river basins as a consequence of energy minimization, *Geophys. Res. Lett.*, *20*, 1583-1586, 1993.
- [35] Inaoka, H., and H. Takayasu, Water erosion as a fractal growth process, *Phys. Rev. E*, *47*, 899-910, 1993.
- [36] Kardar, M., G. Parisi, and Y.-C. Zhang, Dynamic scaling of growing interfaces, *Phys. Rev. Lett.*, *56*, 889-892, 1986.
- [37] Kenyon, P.M., and D.L. Turcotte, Morphology of a delta prograding by bulk sediment transport, *Geol. Soc. Am. Bull.*, *96*, 1457-1465, 1985.
- [38] Kim, J.M., and J.M. Kosterlitz, Growth in a restricted solid-on-solid model, *Phys. Rev. Lett.*, *62*, 2289-2292, 1989.
- [39] Kirchner, J.W., Statistical inevitability of Horton's laws and the apparent randomness of stream channel networks, *Geology*, *21*, 591-594, 1993.

- [40] Kondoh, H., and M. Matsushita, Diffusion-limited aggregations with anisotropic sticking probability: a tentative model for river networks, *J. Phys. Soc. Japan*, *55*, 3289-3292, 1986.
- [41] Kramer, S., and M. Marder, Evolution of river networks, *Phys. Rev. Lett.*, *68*, 205-208, 1992.
- [42] Kucinskas, A.B., D.L. Turcotte, J. Huang, and P.G. Ford, Fractal analysis of Venus topography in Tinatin Planatia and Ovda Regio, *J. Geophys. Res.*, *97*, 13635-13641, 1992.
- [43] La Barbera, P., and R. Rosso, On the fractal dimension of stream networks, *Water Resour. Res.*, *25*, 735-741, 1989.
- [44] Leheny, R.L., S.R. Nagel, Model for the evolution of river networks, *Phys. Rev. Lett.*, *71*, 1470-1473, 1993.
- [45] Leopold, L.B., M.G. Wolman, and J.P. Miller, *Fluvial Processes in Geomorphology*, Freeman, San Francisco, Calif., 1964.
- [46] Leopold, L.B., and T. Maddock Jr., The hydraulic geometry of stream channels and some physiographic implications, *U.S. Geol. Surv. Prof. Paper 252*, 1953.
- [47] Loughridge, M.S., Relief map of the earth's surface, *EOS, Trans. Am. Geophys. Union*, *67*, 121, 1986.
- [48] Luk, S.-H., Variability of rainwash erosion within small sample areas, in *Space and Time in Geomorphology*, edited by C. E. Thorn, pp. 243-268, Allen and Unwin, London, 1982.
- [49] Mandelbrot, B., *The Fractal Geometry of Nature*, W. H. Freeman, New York, 1983.
- [50] Mandelbrot, B., Stochastic models for the earth's relief, the shape and the fractal dimension of coastlines, and the number-area rule for islands, *Proc. Nat. Acad. Sci. U.S.A.*, *72*, 3825-3828, 1975.
- [51] Masek, J.G., and D.L. Turcotte, A diffusion-limited aggregation model for the evolution of drainage networks, *Earth Plan. Sci. Lett.*, *119*, 379-386, 1993.



- [52] Matsushita, M., and S. Ouchi, On the self-affinity of various curves, *Physica D*, *38*, 246-251, 1989.
- [53] Maritan, A., A. Rinaldo, R. Rigon, A. Giacometti, and I. Rodriguez-Iturbe, Scaling laws for river networks, *Phys. Rev. E*, *53*, 1510-1515, 1996.
- [54] Meakin, P., J. Feder, and T. Jossang, Simple statistical models for river networks, *Physica A*, *176*, 409-429, 1991.
- [55] Meyer, L., and D. Nash, eds., *Catastrophic Flooding*, Blackwell Sci., Cambridge, Mass., 1983.
- [56] Milliman, J.D., and J.P.M. Syvitski, Geomorphic/Tectonic control of sediment discharge to the ocean: the importance of small mountainous rivers, *J. Geol.*, *100*, 525-544, 1992.
- [57] Montgomery, D.R., and W.E. Dietrich, Where do channels begin?, *Nature*, *336*, 232-234, 1988.
- [58] Montgomery, D.R., and W.E. Dietrich, Channel initiation and the problem of landscape scale, *Science*, *255*, 826-830, 1992.
- [59] Mulder, T., and J.P.M. Syvitski, Climatic and morphologic relationships of rivers: implications of sea-level fluctuations on river loads, *J. Geol.*, *104*, 509-523, 1996.
- [60] Nash, D.B., Forms of bluffs degraded for different lengths of time in Emmet County, Michigan, USA, *Earth Surf. Processes*, *5*, 331-345, 1980.
- [61] Newman, W.I., and D.L. Turcotte, Cascade model for fluvial geomorphology, *Geophys. J. Int.*, *100*, 433-439, 1990.
- [62] Nikora, V.I., On self-similarity and self-affinity of drainage basins, *Water Resour. Res.*, *30*, 133-137, 1994.
- [63] Ormi, A.R., Temporal variability of a summer shorezone, in *Space and Time in Geomorphology*, edited by C. E. Thorn, pp. 285-313, Allen and Unwin, London, 1982.
- [64] Ossadnik, P., Branch order and ramification analysis of large diffusion-limited-aggregation

- clusters, *Phys. Rev. A*, *45*, 1058-1066, 1992.
- [65] Park, K., and B. Kahng, Exact derivation of the Kardar-Parisi-Zhang equation for the restricted solid-on-solid model, *Phys. Rev. E*, *51*, 796-798, 1995.
- [66] Patton, P.C., and S.A. Schumm, Gully erosion, Northwestern Colorado: A threshold phenomenon, *Geology*, *3*, 88-90, 1975.
- [67] Peckham, S.D., New results for self-similar trees with applications to river networks, *Water Resour. Res.*, *31*, 1023-1029, 1995.
- [68] Peckham, S.D., RiverTools 1.01, electronic software, available at <http://cires.colorado.edu/people/peckham.scott/RT.html>, 1997.
- [69] Phillips, B.C., and A.J. Sutherland, Diffusion models applied to channel degradation, *J. Hyd. Res.*, *25*, 179-191, 1986.
- [70] Pierce, K.L., and S.M. Colman, Effect of height and orientation (microclimate) on geomorphic degradation rates and processes, late-glacial terrace scarps in central Idaho, *Bull. Geol. Soc. Am.*, *97*, 869-885, 1986.
- [71] Plotnick, R.E., and K. Prestegard, Fractal analysis of geologic time series, in *Fractals in Geography*, edited by L. De Cola and S. Lam, pp. 193-210, Prentice-Hall, Englewood Cliffs, Cal., 1993.
- [72] Rodriguez-Iturbe, I., E. Ijjasz-Vasquez, R.L. Bras, and D.G. Tarboton, Power-law distributions of discharge mass and energy in river basins, *Water Resour. Res.*, *28*, 1089-1093, 1992.
- [73] Sadler, P.M., Sediment accumulation rates and the completeness of stratigraphic sections, *J. Geol.*, *89*, 569-584, 1981.
- [74] Sayles, R.S., and T.R. Thomas, Surface topography as a non-stationary random process, *Nature*, *271*, 431-434, 1978.
- [75] Schmidt, K.-H., Regional variation of mechanical and chemical denudation, upper Colorado

- River basin, U.S.A., *Earth Surf. Processes*, 10, 497-508, 1985.
- [76] Schumm, S.A., Evolution of drainage systems and slopes on badlands at Perth Amboy, New Jersey, *Geol. Soc. Am. Bull.*, 67, 597-696, 1956.
- [77] Shreve, R.L., Statistical law of stream numbers, *J. Geol.*, 74, 17-37, 1966.
- [78] Smith, T.R., and F.P. Bretherton, Stability and the conservation of mass in drainage basin evolution, *Water Resour. Res.*, 8, 1506-1529, 1972.
- [79] Sornette, D., and Y.-C. Zhang, Non-linear Langevin model of geomorphic erosion processes, *Geophys. J. Int.*, 113, 382-386, 1993.
- [80] Stark, C.P., An invasion percolation model of drainage network evolution, *Nature*, 352, 432-425, 1991.
- [81] Stark, C.P., Cluster growth modeling of plateau erosion, *J. Geophys. Res.*, 99, 13957-13969, 1994.
- [82] Tarboton, D.G., R.L. Bras, and I. Rodriguez-Iturbe, The fractal nature of river networks, *Water Resour. Res.*, 24, 1317-1322, 1988.
- [83] Tarboton, D.G., R.L. Bras, and I. Rodriguez-Iturbe, Scaling and elevation in river networks, *Water Resour. Res.*, 25, 2037-2051, 1989.
- [84] Tokunaga, E., Ordering of divide segments and law of divide segment numbers, *Trans. Jpn. Geomorphol. Union*, 5, 71-77, 1984.
- [85] Turcotte, D.L., A fractal interpretation of topography and geoid spectra on the earth, Moon, Venus, and Mars, *J. Geophys. Res.*, 92, 597-601, 1987.
- [86] Turcotte, D.L., *Fractals and Chaos in Geology and Geophysics*, Cambridge Univ. Press, New York, 1992.
- [87] United States Geological Survey, Digital Elevation Models, National Mapping Program Tech-

- nical Instructions, Data Users Guide 5, U.S. Geological Survey, Second Printing (Revised), Reston, Virginia, 1990.
- [88] Vening Meinesz, F.A., A remarkable feature of the earth's topography, *Proc. K. Ned. Akad. Wet. Ser. B*, 54, 212-228, 1951.
- [89] Voss, R., Fractals in nature: From characterization to simulation, in *The Science of Fractal Images*, edited by H. Peitgen and D. Saupe, pp. 22-70, Springer-Verlag, New York, 1988.
- [90] Wallace, R.E., Profiles and ages of young fault scarps, north-central Nevada, *Geol. Soc. Am. Bull*, 88, 1267-1281, 1977.
- [91] Weissel, J.K., L.F. Pratson, and A. Malinverno, The length-scaling properties of topography, *J. Geophys. Res.*, 99, 13997-14012, 1994.
- [92] Willgoose, G., A statistic for testing the elevation characteristics of landscape evolution models, *J. Geophys. Res.*, 99, 13987-13996, 1994.
- [93] Willgoose, G., R.L. Bras, and I. Rodriguez-Iturbe, A coupled channel network growth and hillslope evolution model 1. theory, *Water Resour. Res.*, 27, 1671-1684, 1991.
- [94] Wolman, M.G., and R. Gerson, Relative scales of time and effectiveness of climate in watershed geomorphology, *Earth Surf. Processes*, 3, 189-208, 1978.

FIG. 1. Illustration of the topographic evolution with diffusion. (a) The initial topographic profile at some time  $t$ , given by a Gaussian, (b) the Laplacian of the initial topography, and (c) the initial topography (dashed line) and final topography (solid line) after a small increment of time according to the diffusion equation. The topography aggrades where the surface was concave and is eroded where the surface was concave down. After *Barabasi and Stanley* [1995].

FIG. 2. Illustration of the topographic evolution with the nonlinear term of equation 11. (a) The initial topographic profile at some time  $t$ , given by a Gaussian, (b) the nonlinear term of the initial topography, and (c) the initial topography (dashed line) and final topography (solid line) after a small increment of time. The final surface is skewed so that it is no longer Gaussian and has more area in lowlands than the initial profile. After *Barabasi and Stanley* [1995].

FIG. 3. Shaded relief image of topography produced with the restricted solid-on-solid (RSOS) model.

FIG. 4. Average power spectrum  $S$  as a function of wave number  $k$  for one-dimensional transects of the surface generated with the RSOS model. A least-square fit to the logarithms of the ordinate and abscissa yield a slope of  $-1.81$  indicating that  $S(k) \propto k^{-1.81}$ .

FIG. 5. (a) Probability density function of elevations of the surface (hypsoetry) produced by the RSOS model. (b) Probability density function of the Kentucky River basin. (c) Probability density function of the Mississippi River basin. All three exhibit a significant skew such that lowlands (topography below the median elevation) make up a larger fraction of the total area than highlands.

FIG. 6. Cumulative hypsometric curves (dots), the fraction of area above an elevation normalized by the maximum elevation, for (a) Africa, (b) North America, and (c) South America, from the data of *Harrison et al.* [1983]. The line accompanying each plot is the least squares fit to a lognormal distribution for each continent.

FIG. 7. Drainage networks analyzed: (a) Kumaun, (b) Loess Plateau, Shanxi Province, (c) Schoharie Creek, (d) Nepal, (e) Kentucky River, (f) Mississippi River, (g) Bhutan

FIG. 8. Plot of average number of streams  $N$  of a given Strahler order as a function of the average drainage area  $A$  for that Strahler order for each of the seven river basins. The plots are offset from one another so that they may be placed on the same graph. The plots correspond, from top to bottom, to the river basins in (a) through (g) of Figure 7, respectively. The data indicate that  $N \approx A^{-1}$ .

FIG. 9. Plot of average main channel length  $L$  of a given Strahler order as a function of the average drainage area  $A$  for that Strahler order for each of the seven river basins. The plots are offset from one another so that they may be placed on the same graph. The plots correspond, from top to bottom, to the river basins in (a) through (g) of Figure 7, respectively. The data indicate that  $L \approx A^q$  with  $q \approx 0.5-0.6$ .

FIG. 10. Plot of average along-channel slope  $S$  of a given Strahler order as a function of the average drainage area  $A$  for that Strahler order for each of the seven river basins. The plots are offset from one another so that they may be placed on the same graph. The plots correspond, from top to bottom, to the river basins in (a) through (g) of Figure 7, respectively. The data indicate that  $S \approx A^{-\frac{3}{8}}$ .

FIG. 11. Plot of average basin relief  $R$  for a given Strahler order as a function of the average drainage area  $A$  for that Strahler order for each of the seven river basins. The plots are offset from one another so that they may be placed on the same graph. The plots correspond, from top to bottom, to the river basins in (a) through (g) of Figure 7, respectively. The data indicate that  $R \approx A^{-s}$  with  $s$  ranging from  $1/5$  to  $1/3$ .

FIG. 12. Plot of average basin area  $A$  of a given Strahler order as a function of the Strahler order  $o$  for each of the seven river basins. Note the log-linear scale. The plots are offset from one another so that they may be placed on the same graph. The data indicate that  $R_A$  is constant and equal to approximately  $10^{\frac{2}{3}} \approx 4.6$ .

FIG. 13. Plot of the Tokunaga ratio  $T_k$  a function of the Strahler order  $k$  for each of the seven river basins. Note the log-linear scale. The plots are offset from one another so that they may be placed on the same graph. The data indicate that  $T_k \propto u^k$  with  $u \approx 10^{0.4} \approx 2.5$ .

FIG. 14. Greyscale plot of the elevation of the model river network when (a) 1/8, (b) 1/4, (c) 1/2, and (d) all of the grid points of the 64 x 64 lattice has become channelized. The elevations are mapped to brightness scale with a gamma function with a coefficient of 2.0.

FIG. 15. Model river networks produced after all of the grid points have become channels. The width of the river is proportional to its order. The fully deterministic model is shown in (a). A model run where the diffusivity is allowed to have a stochastic variation with a standard deviation 10% of the mean is shown in (b).

FIG. 16. Plot of average number of streams  $N$  of a given Strahler order as a function of the average drainage area  $A$  for that Strahler order for three model river basins. The plots are offset from one another so that they may be placed on the same graph. The plots correspond, from top to bottom, to the model river basins produced with a deterministic 64 x 64 model run until all of the grid points were channels, a deterministic 64 x 64 model run until 50% of the grid points were channels, and a 64 x 64 model with small (10%) stochastic variations in the diffusivity run until all of the grid points were channels. The data indicate that  $N \approx A^{-1}$ , similar to that observed for real river networks.

FIG. 17. Plot of average main channel length  $L$  of a given Strahler order as a function of the average drainage area  $A$  for that Strahler order for each of the three model river basins. The plots are in the same order as Figure 16. The data indicate that  $L \approx A^q$  with  $q \approx 0.5=0.6$ , similar to that observed for real river networks.

FIG. 18. Plot of average along-channel slope  $S$  of a given Strahler order as a function of the average drainage area  $A$  for that Strahler order for each of the three model river basins. The plots are in the same order as Figure 16. The data indicate that  $S \approx A^{-0.3}$ , a slightly larger exponent than that observed in real river basins.

FIG. 19. Plot of average basin relief  $R$  for a given Strahler order as a function of the average drainage area  $A$  for that Strahler order for each of the three model river basins. The data indicate that  $R \approx A^{-s}$  with  $s \approx 0.3$ , consistent with observations.

FIG. 20. Plot of average basin area  $A$  of a given Strahler order as a function of the Strahler order  $o$  for each of the three model river basins. Note the log-linear scale. The data indicate that  $R_A$  is constant and equal to approximately  $10^{0.75} \approx 5.6$ , slightly larger than the observed value of 4.6.

FIG. 21. Plot of the Tokunaga ratio  $T_k$  a function of the Strahler order  $k$  for each of the three model river basins. Note the log-linear scale. The data indicate that  $T_k \propto u^k$  with  $u \approx 10^{0.5} \approx 3.2$ .

FIG. 22. Probability density function of the model river basin of Figure 17a. The skew in this p.d.f. is directly analagous to that of the Kentucky and Mississippi River basins of Figure 5b and 5c, respectively, and can be associated with the dependence of diffusivity on elevation.

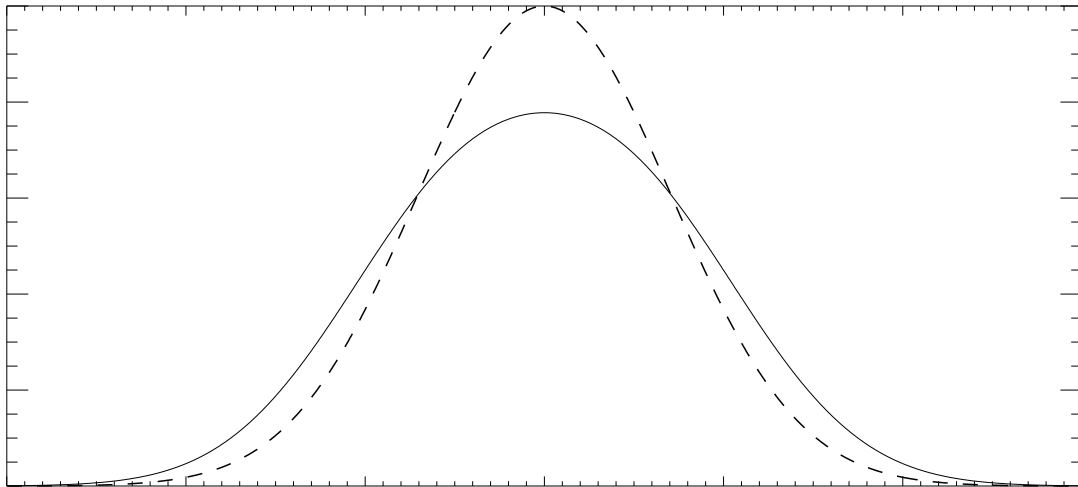
FIG. 23. Evolution of the hypsometric curves for the model river basin for the four instants of time illustrated in Figure 14. Increasing time results in a smoother hypsometric curve.

FIG. 24. Observed evolution of the hypsometric curves from field observations at Perth Amboy, New Jersey [*Schumm*, 1956].

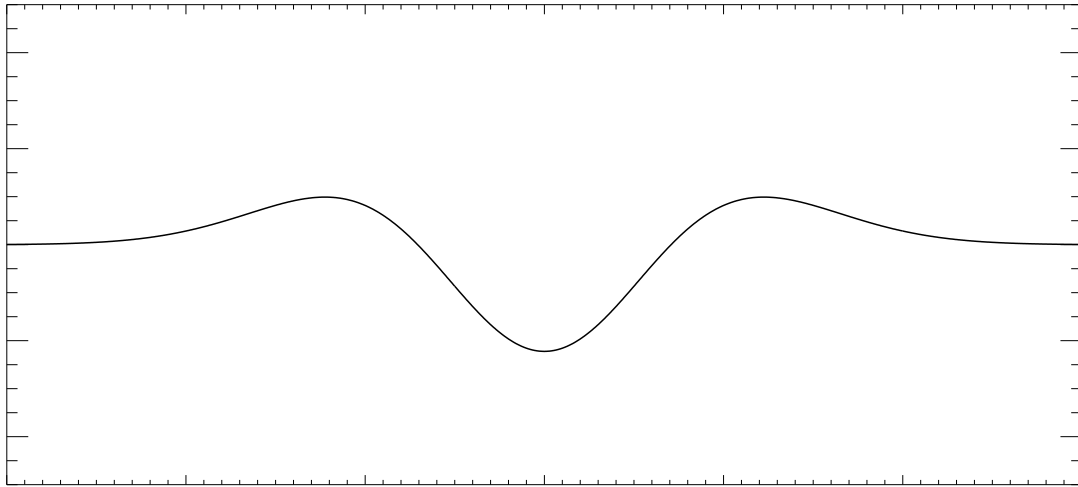


x

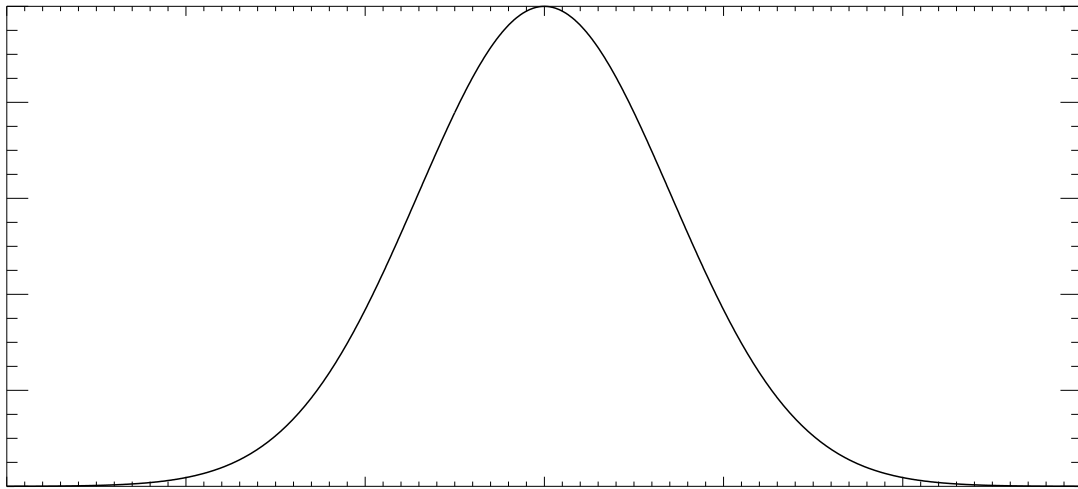
$h(x, t + \Delta t)$



$D_0 \nabla^2 h$

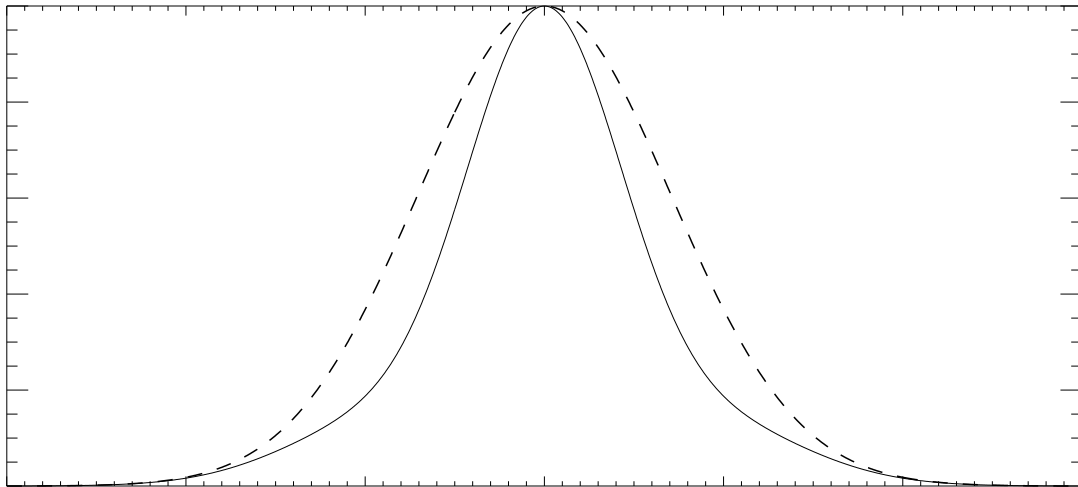


$h(x, t)$

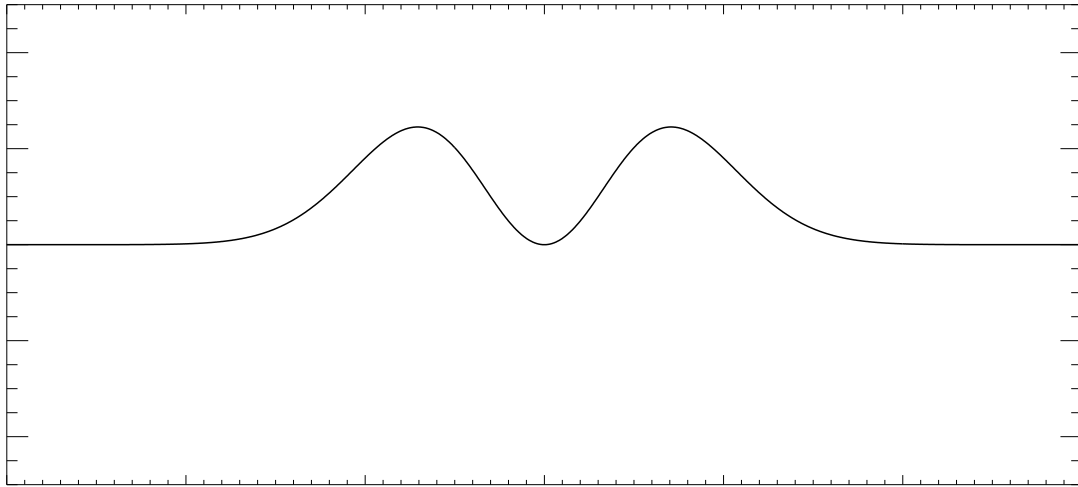


x

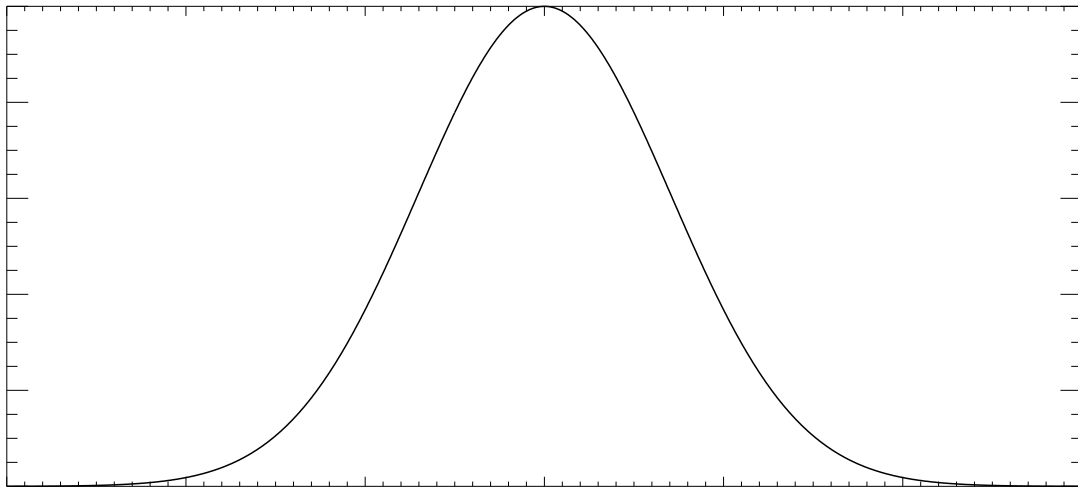
$$h(x, t + \Delta t)$$

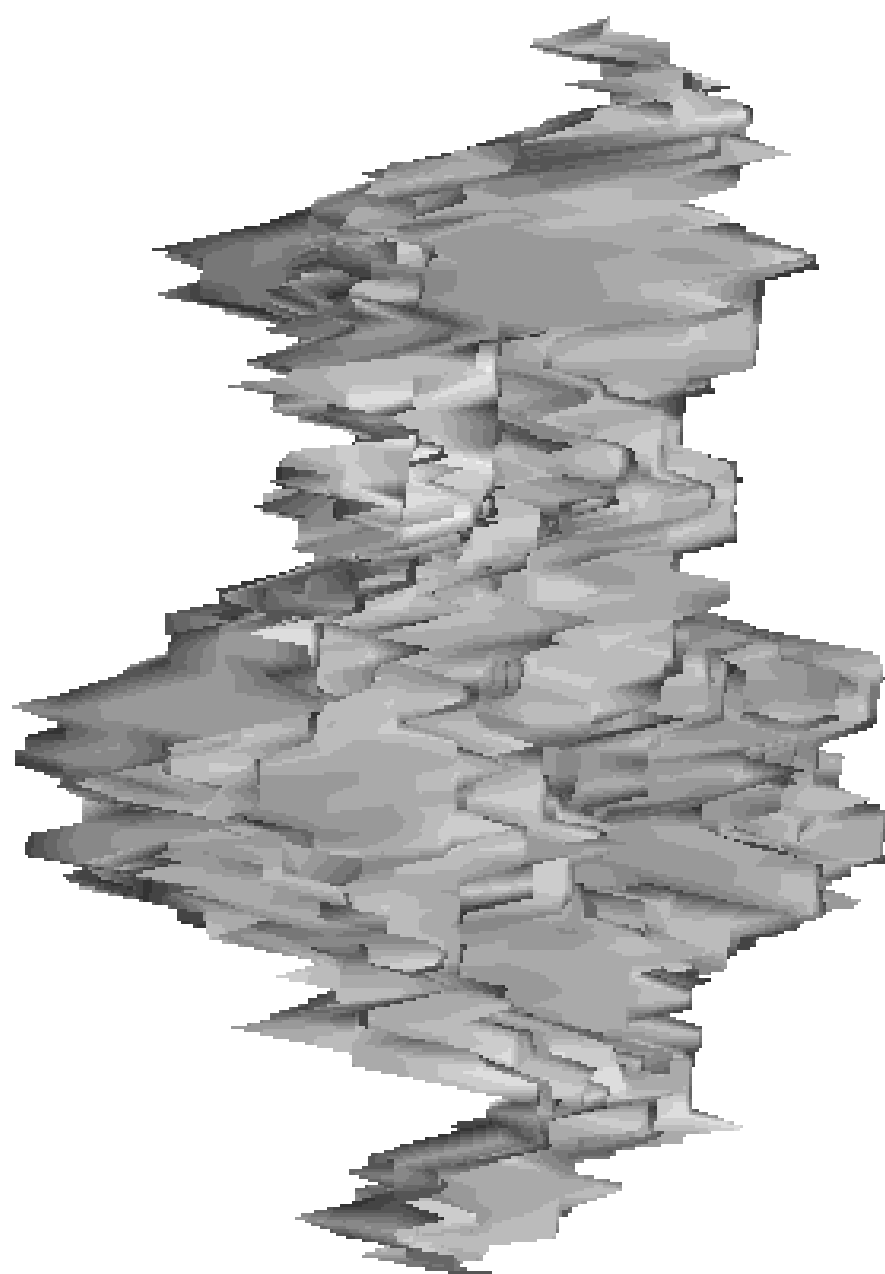


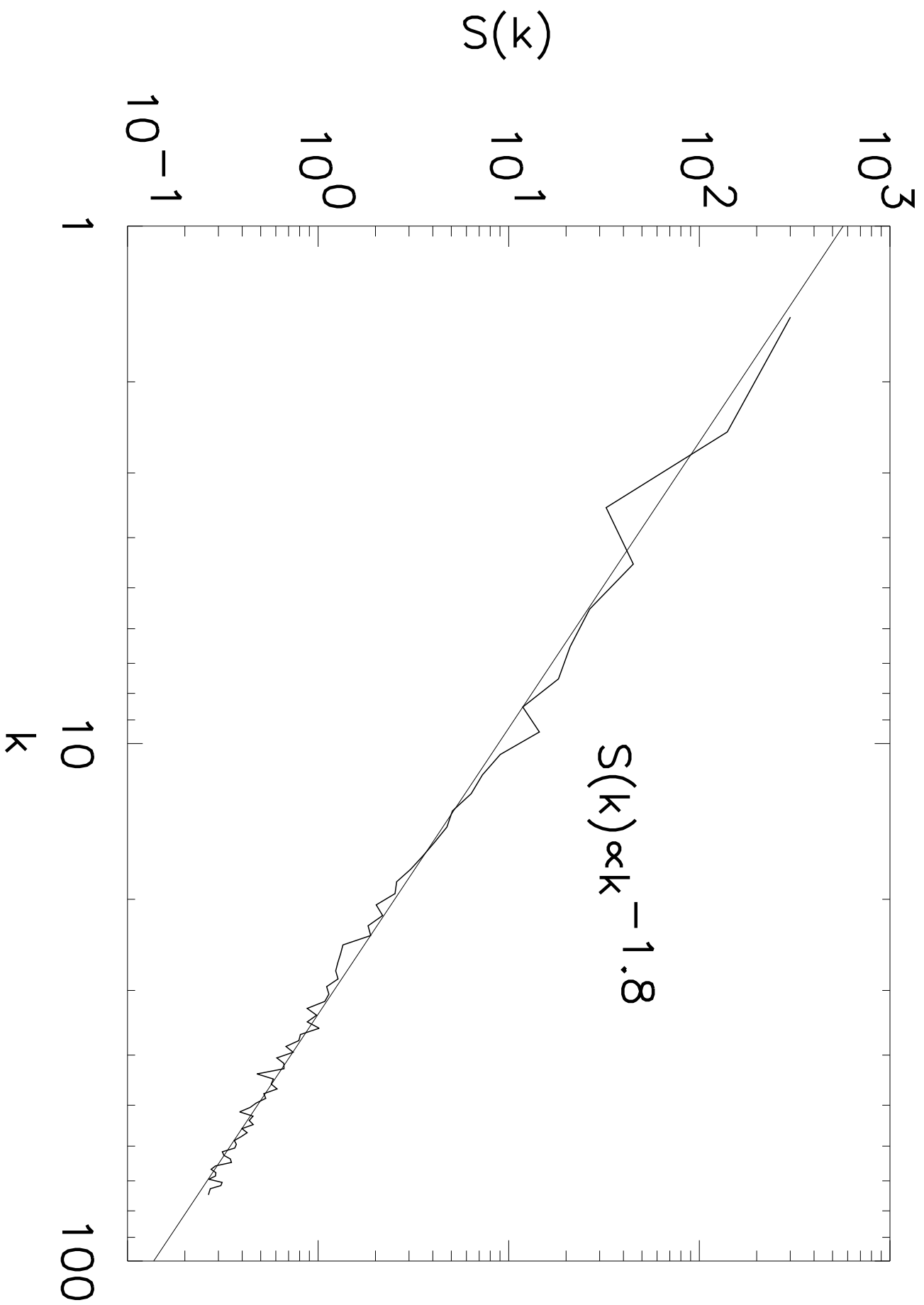
$$D_x(\nabla h)^2$$

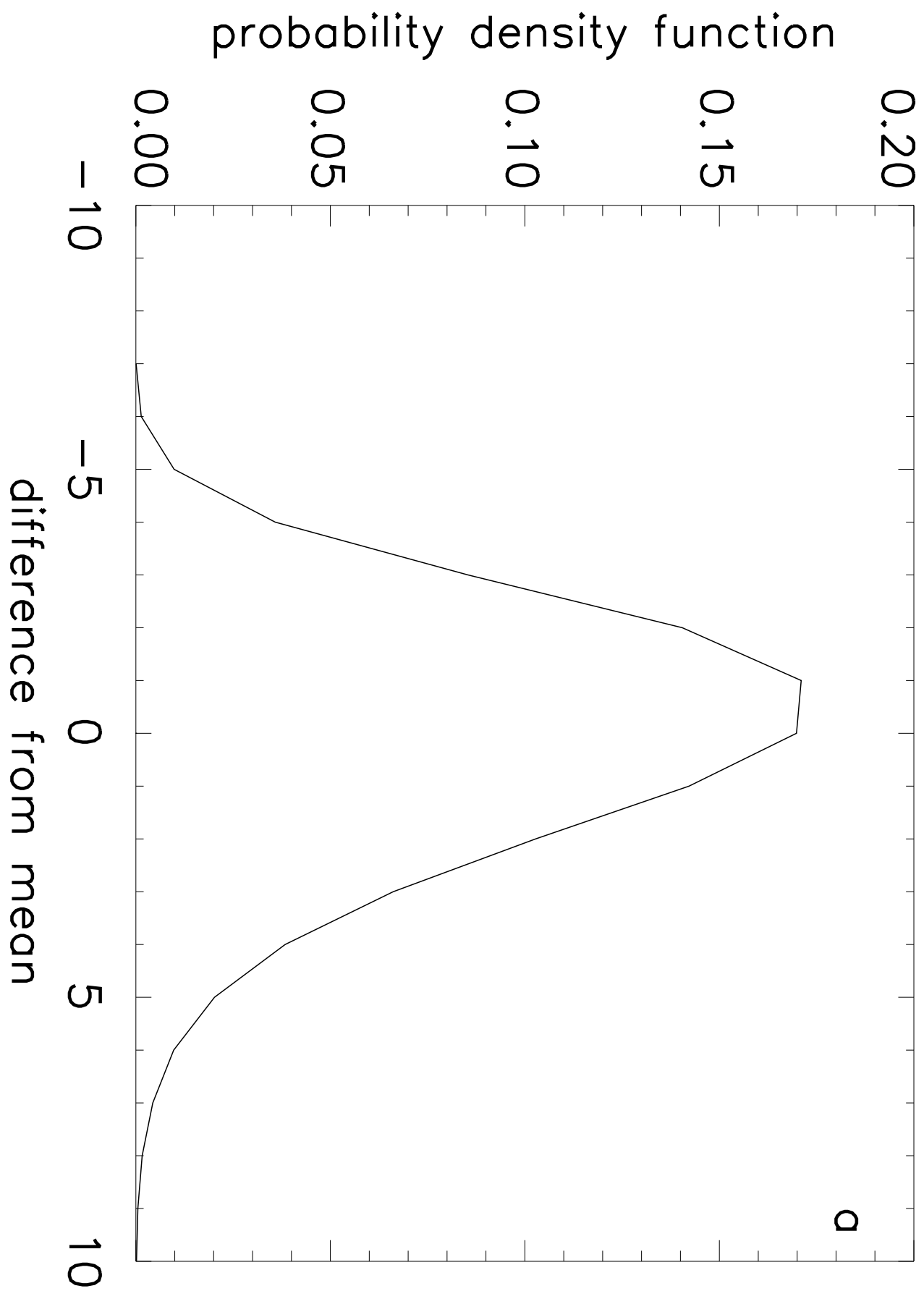


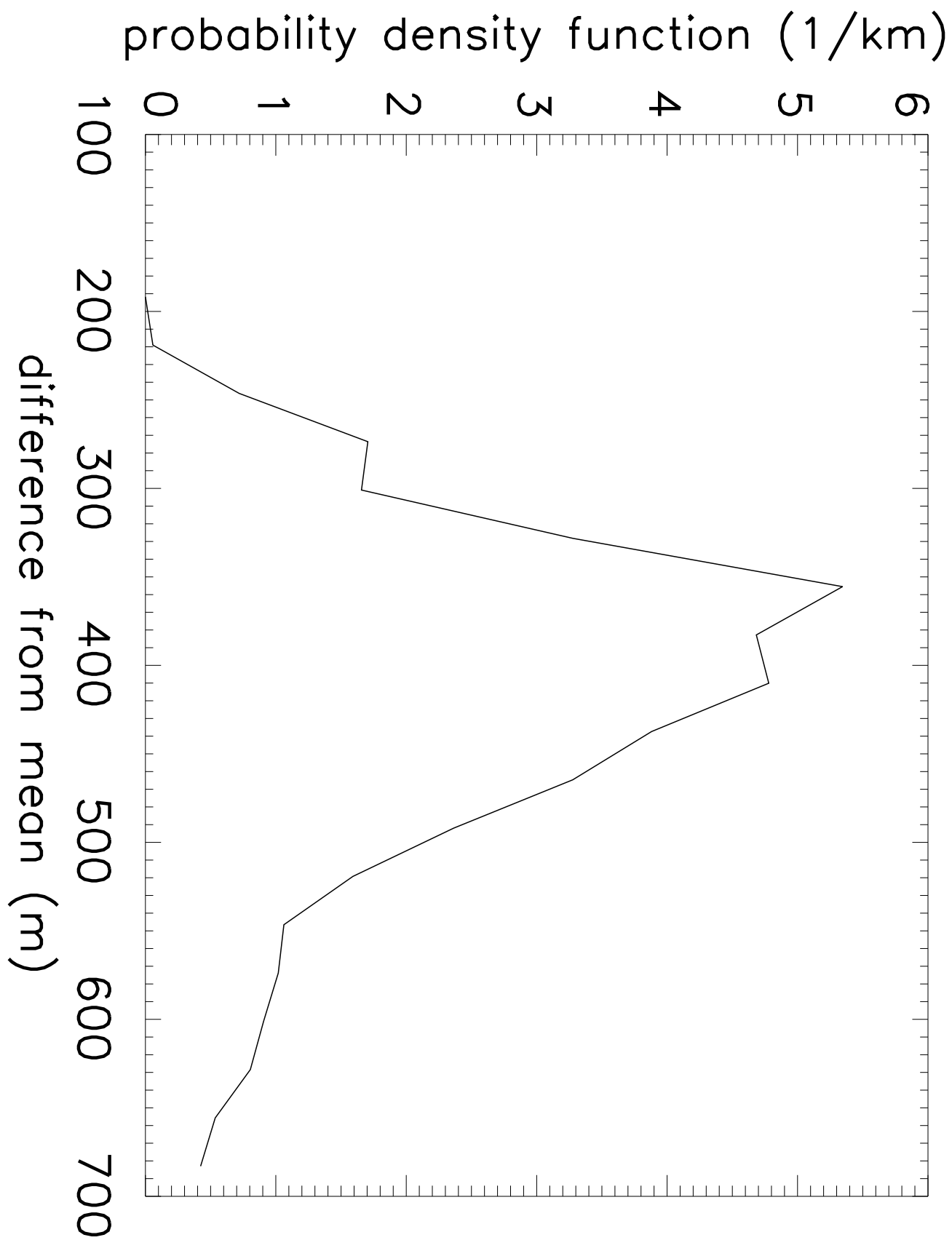
$$h(x, t)$$

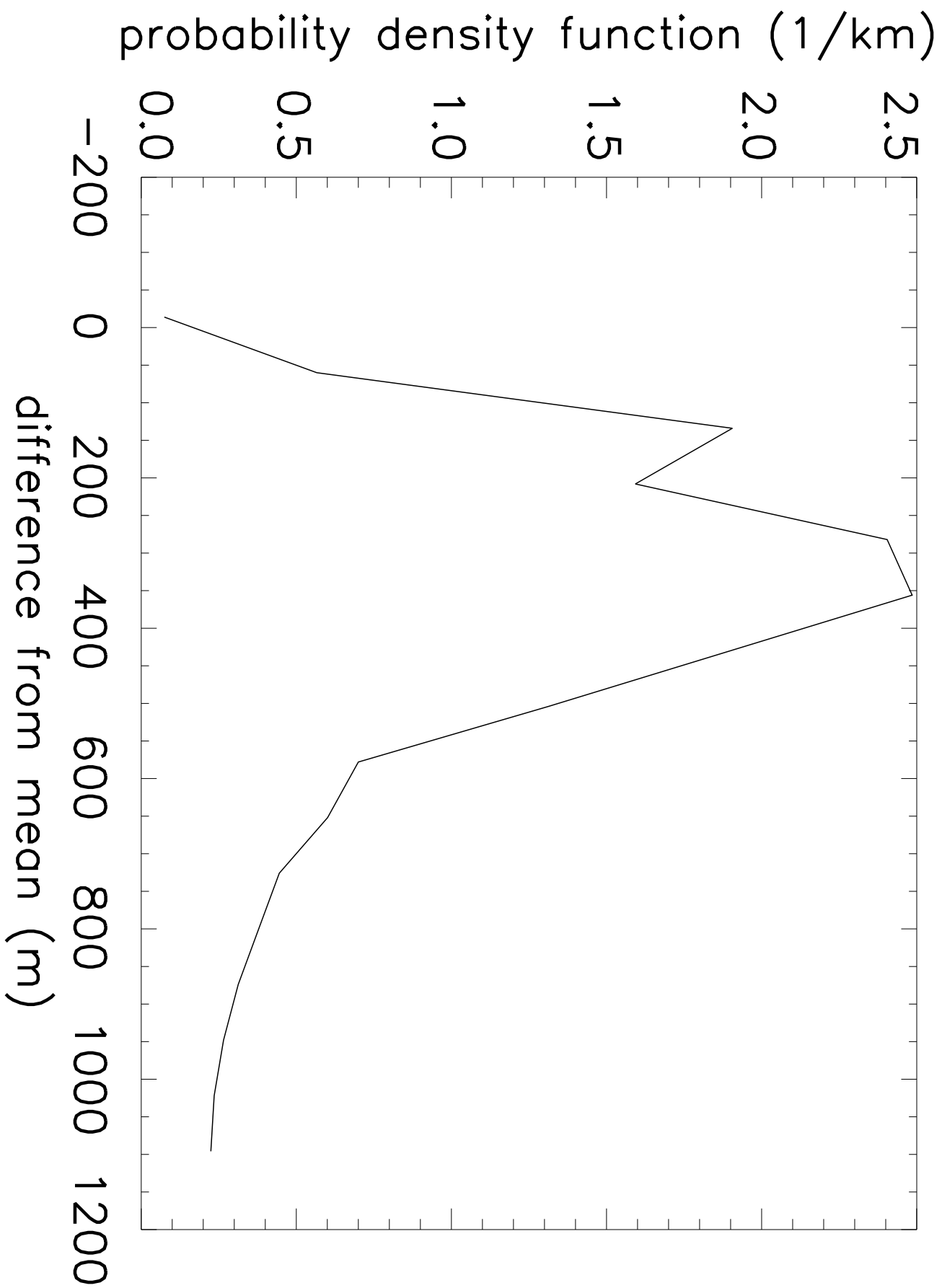


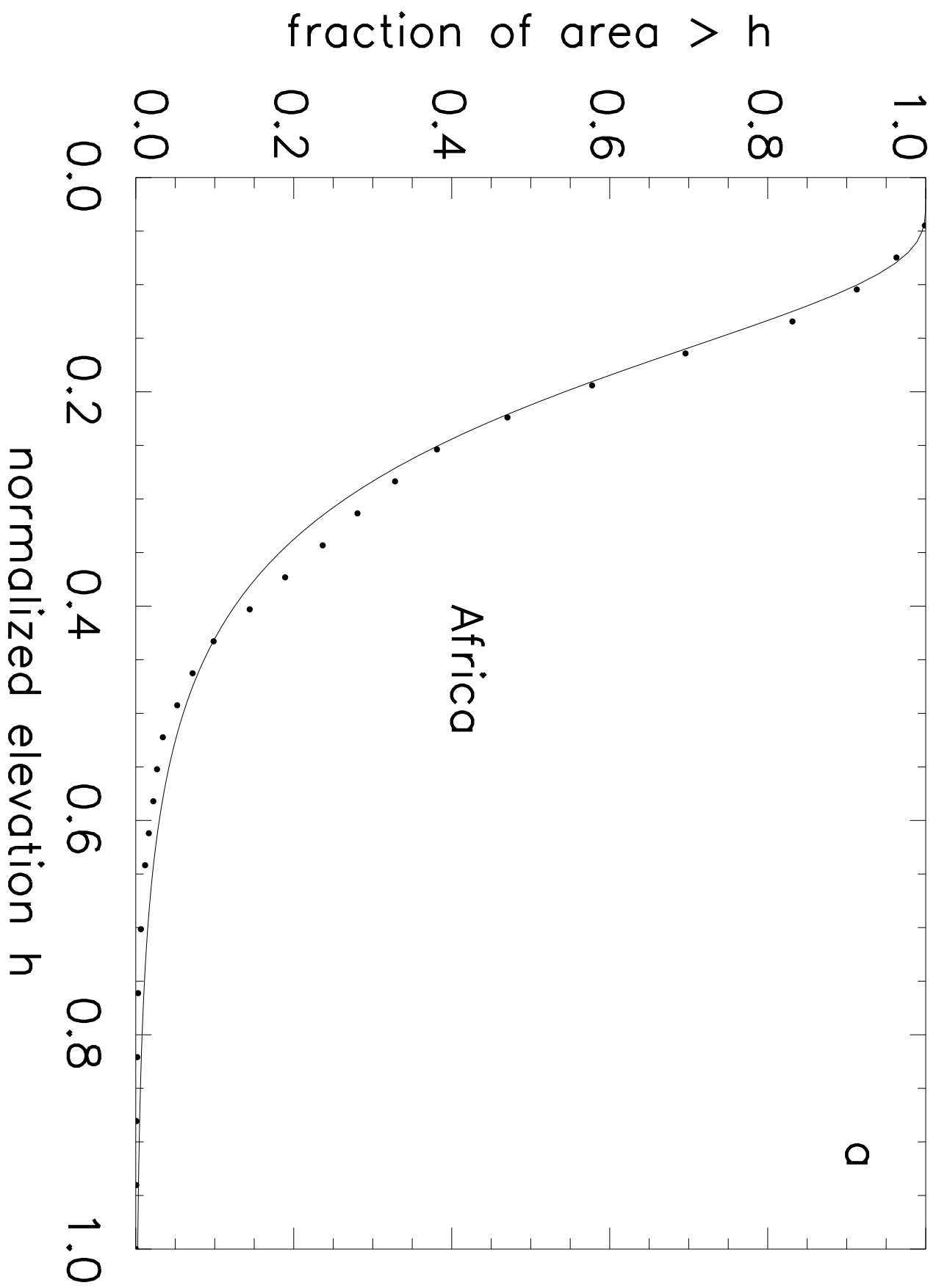




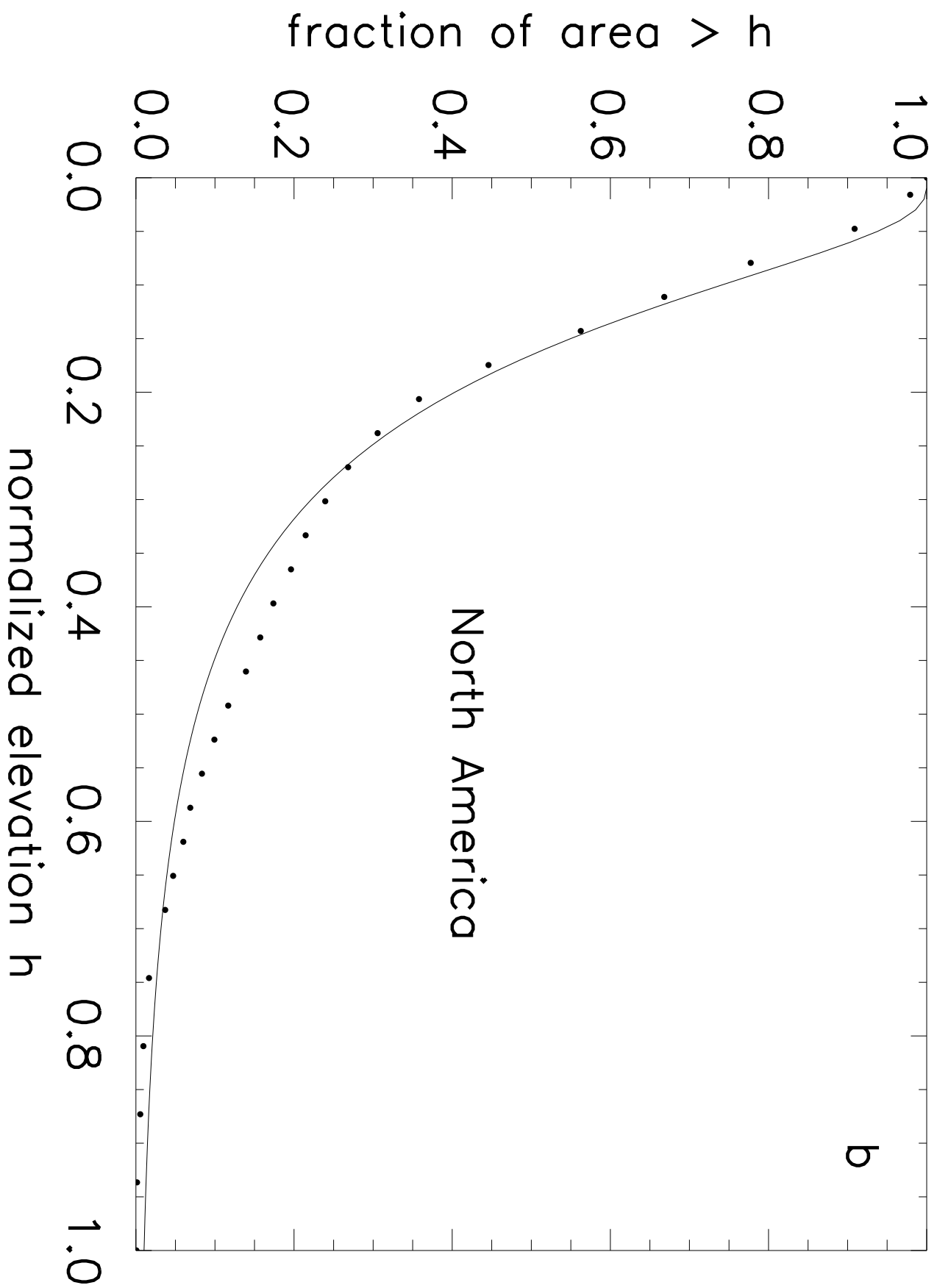


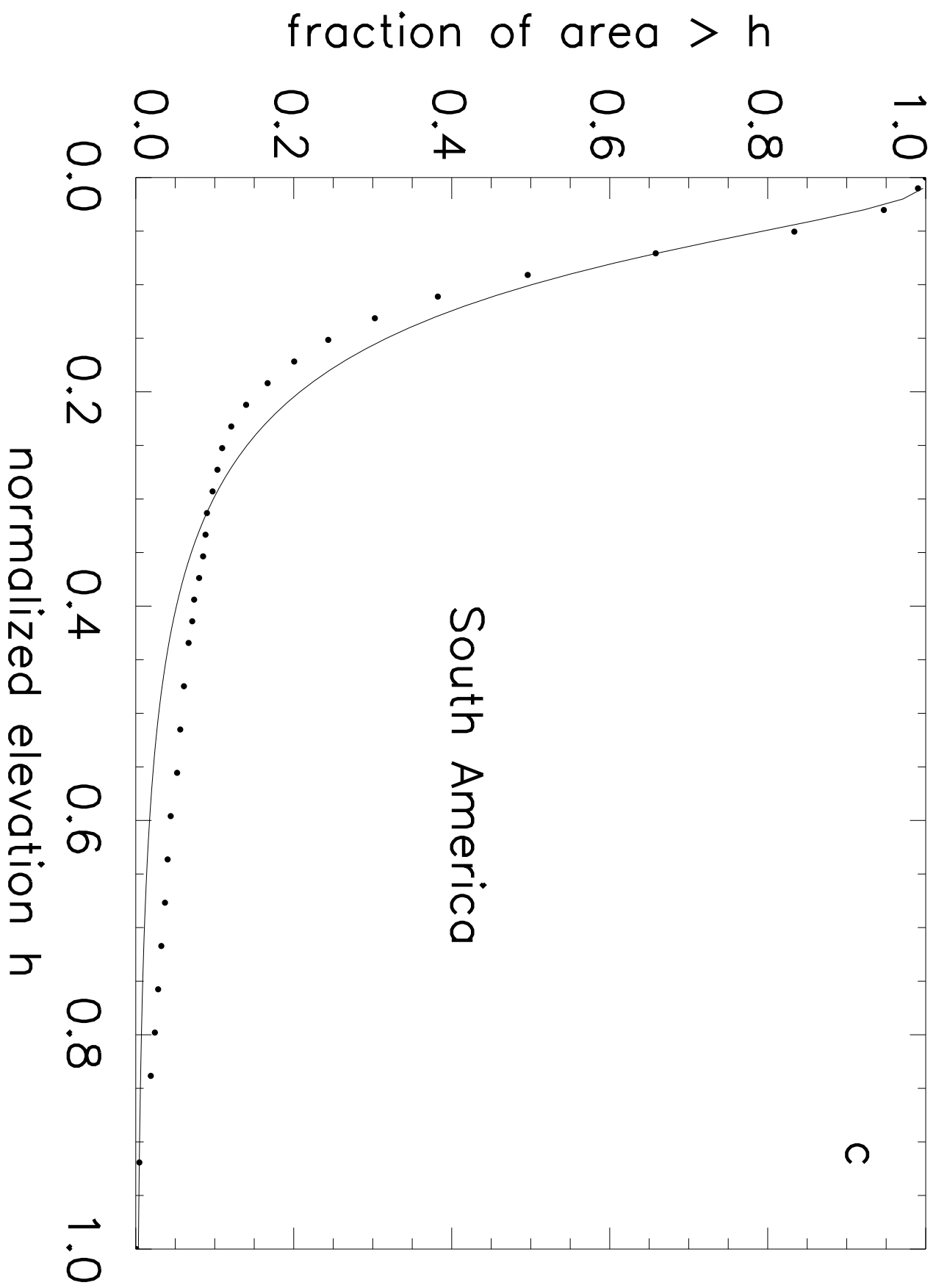




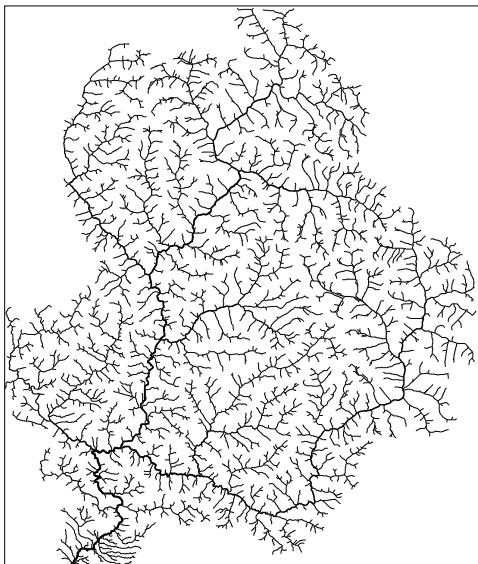




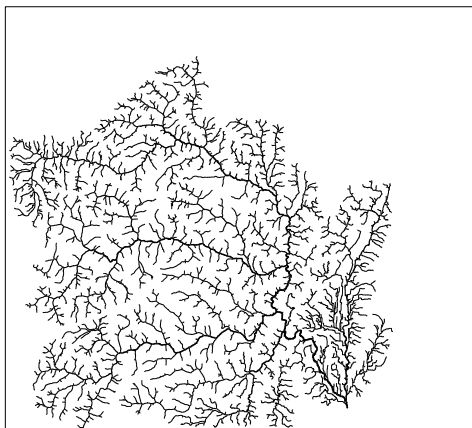




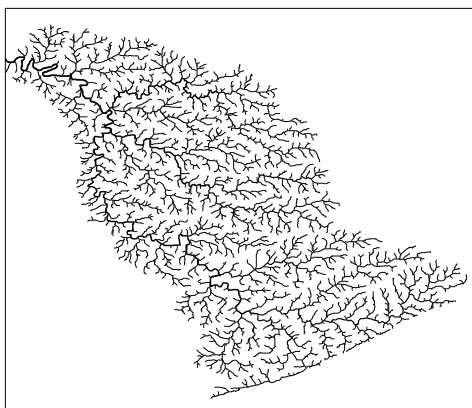
**a**



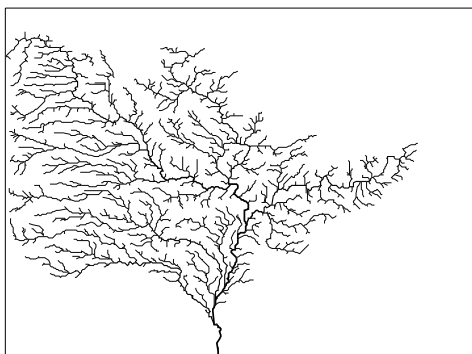
**d**



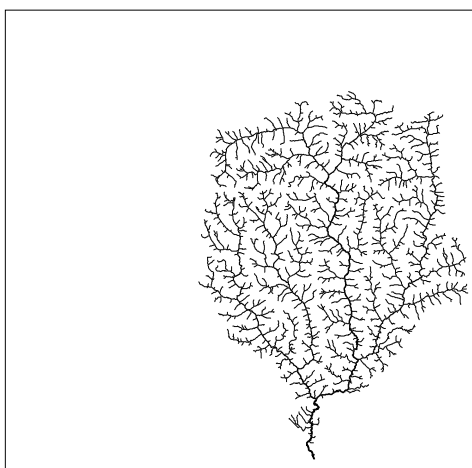
**e**



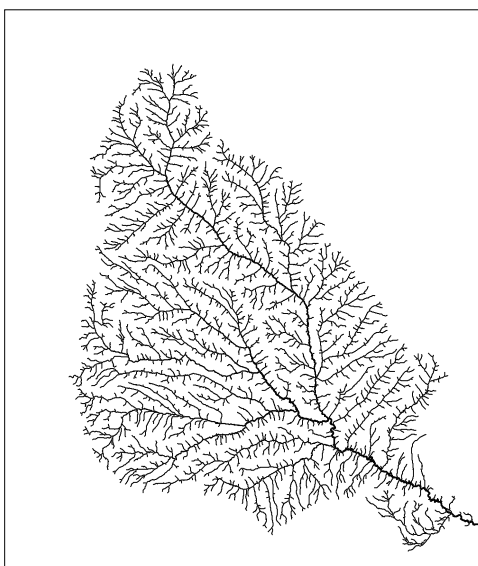
**f**



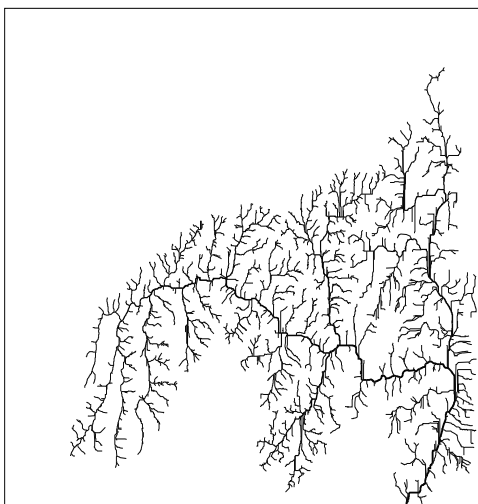
**g**

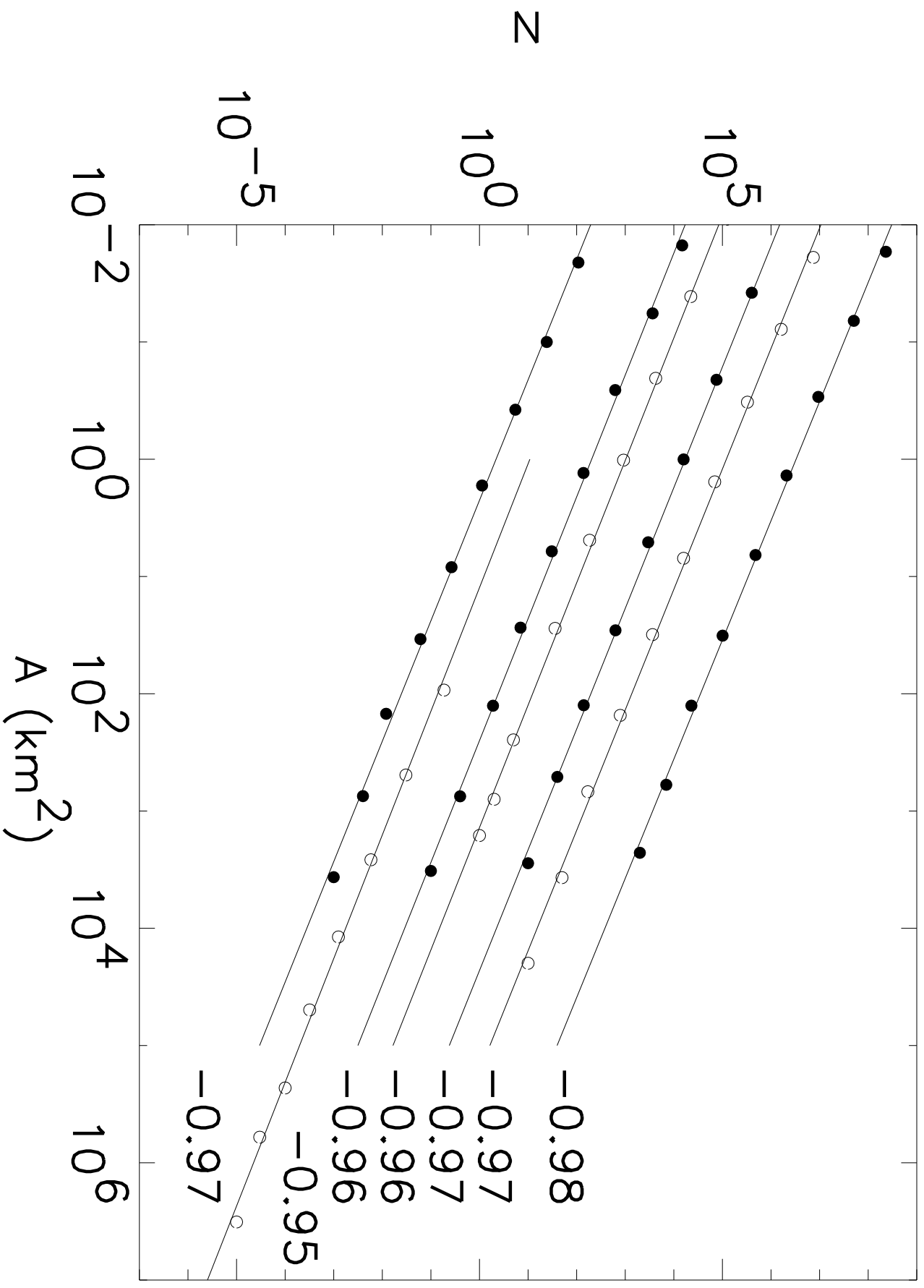


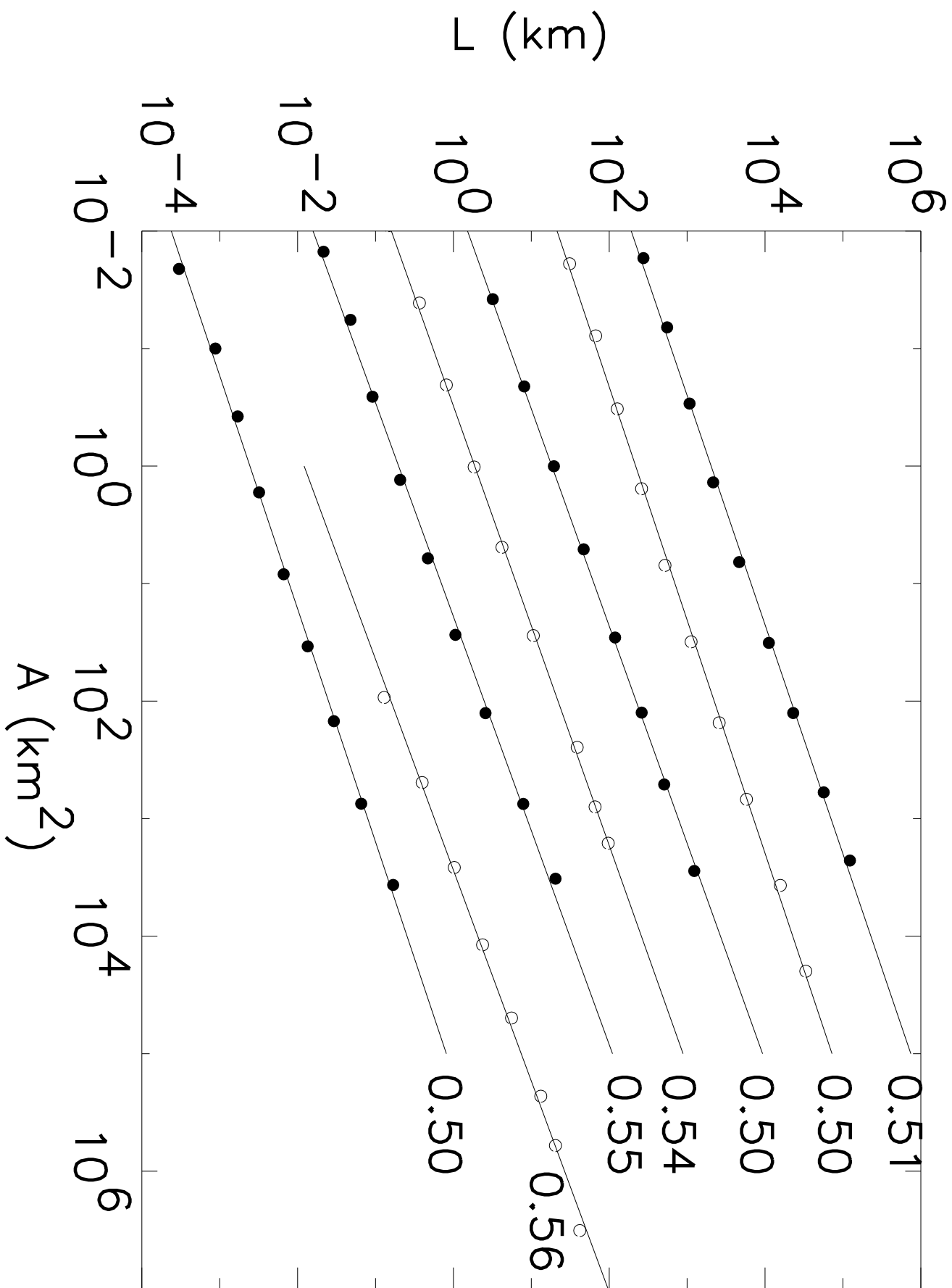
**b**

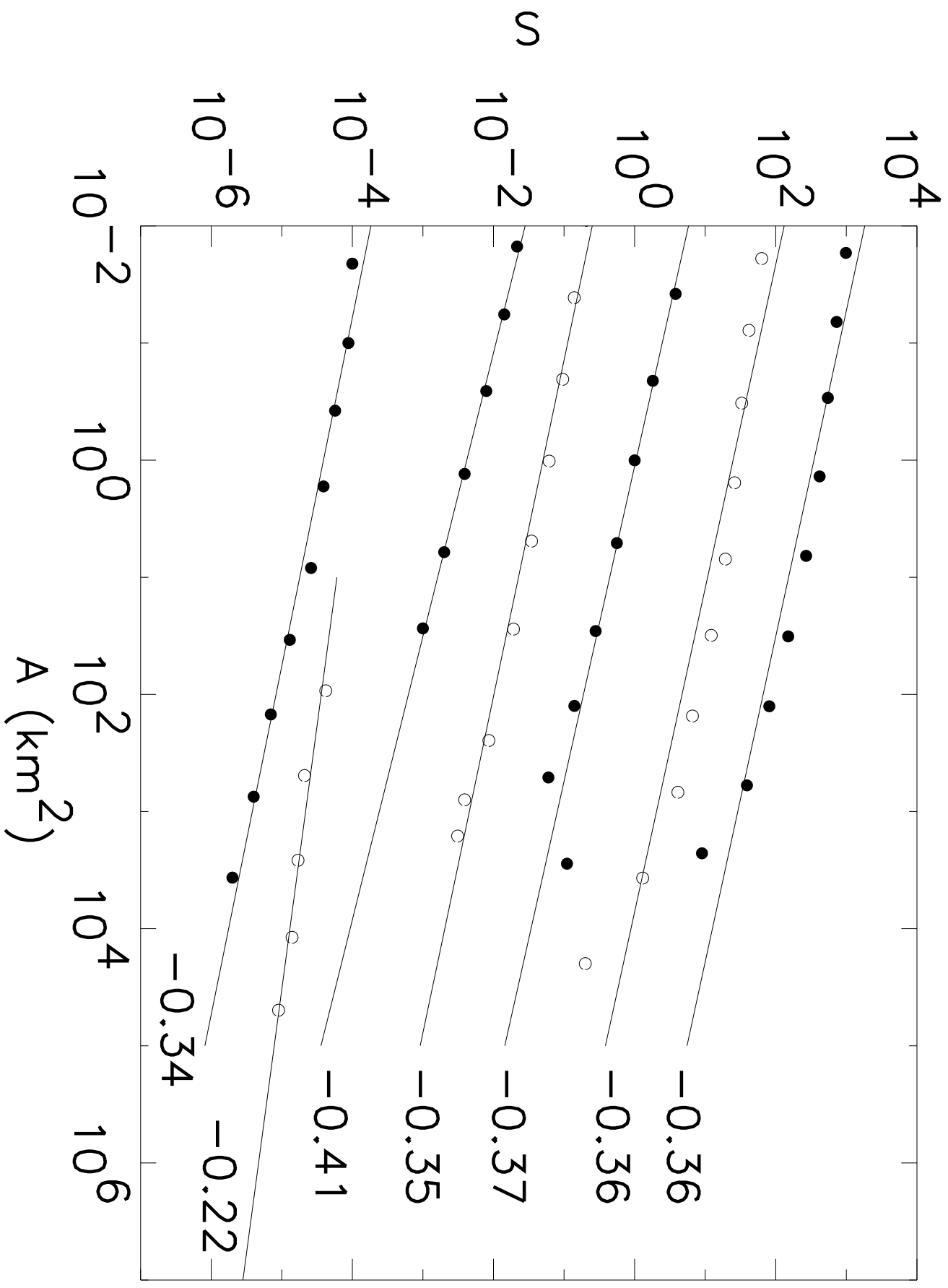


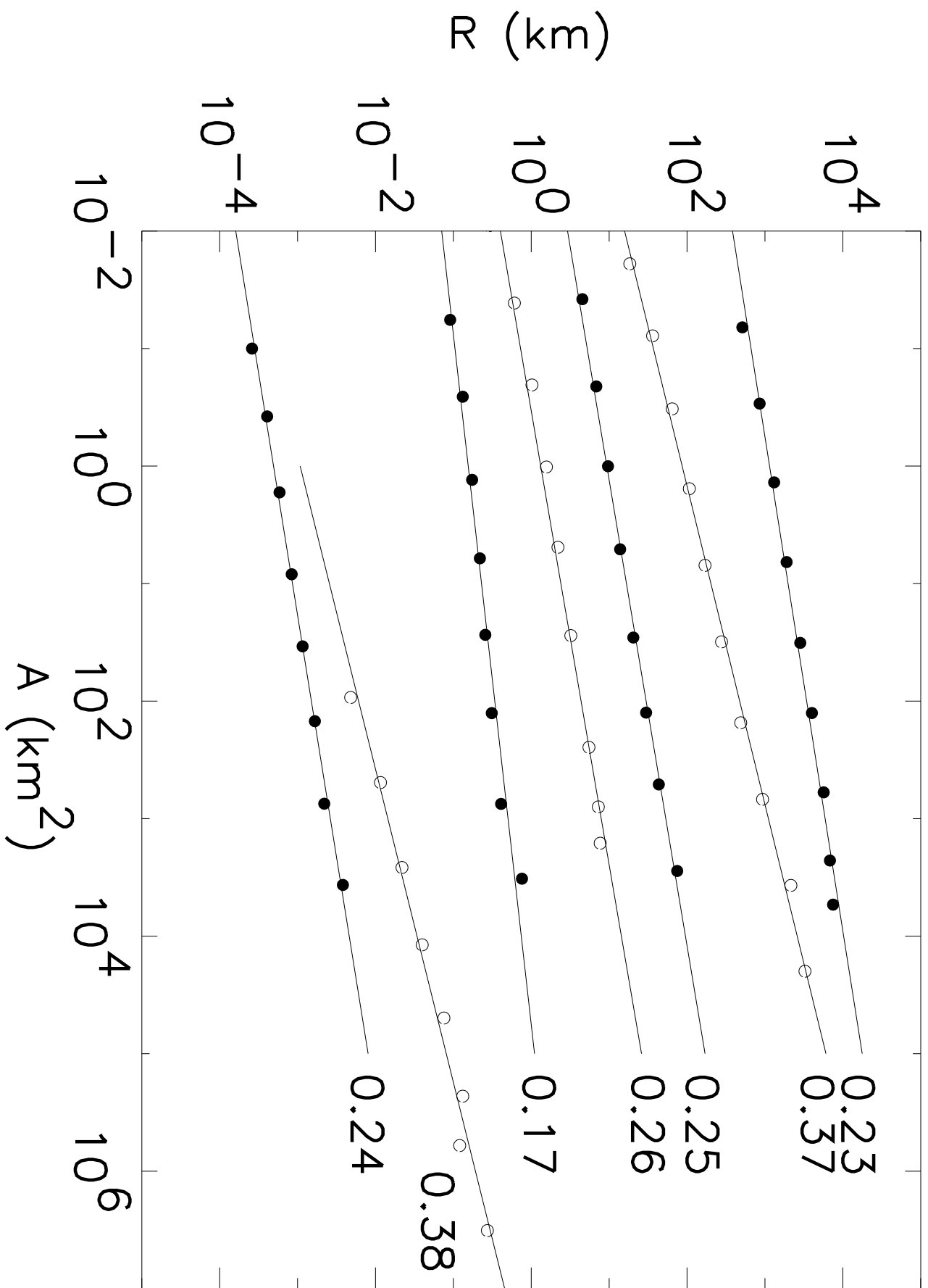
**c**

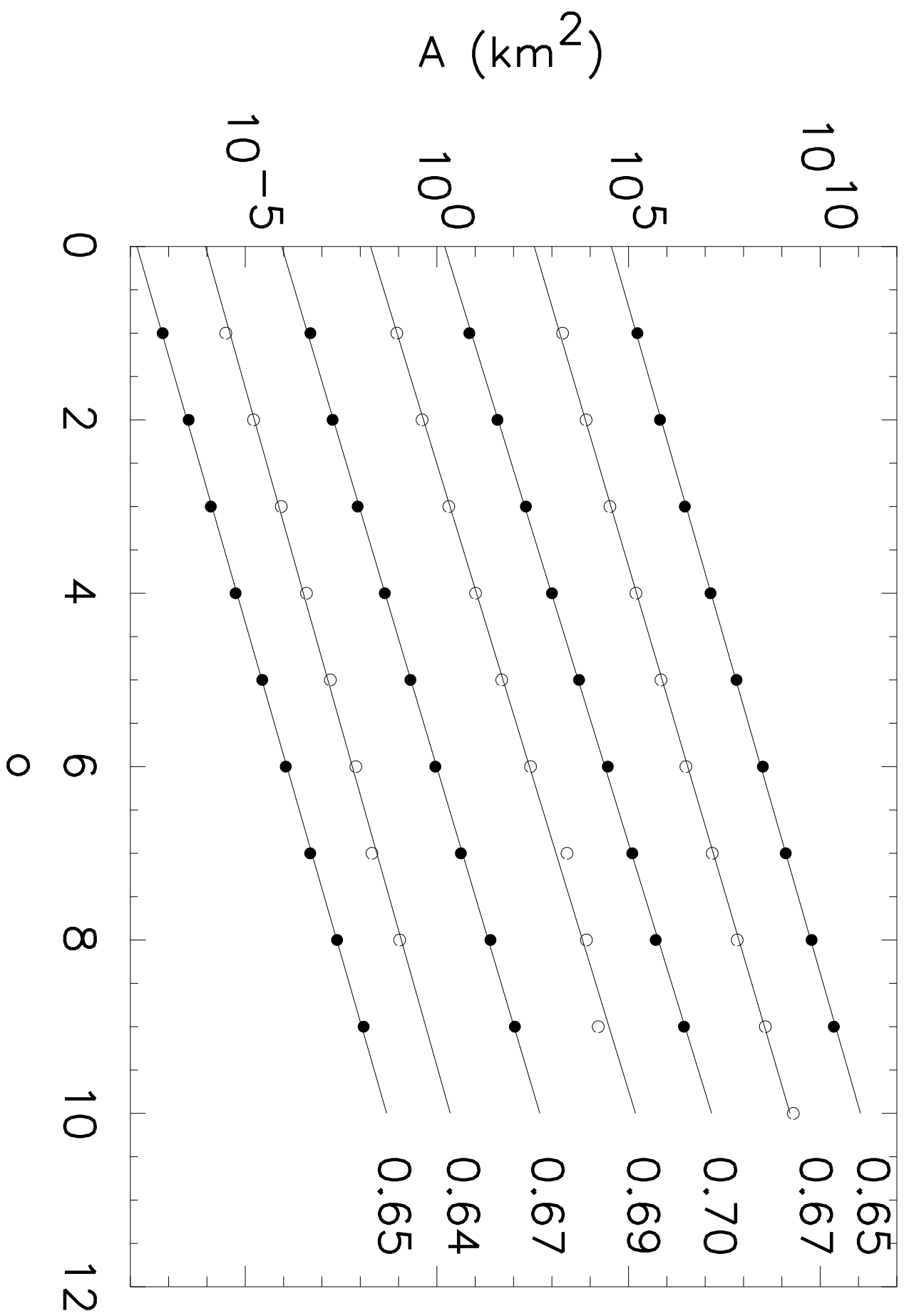




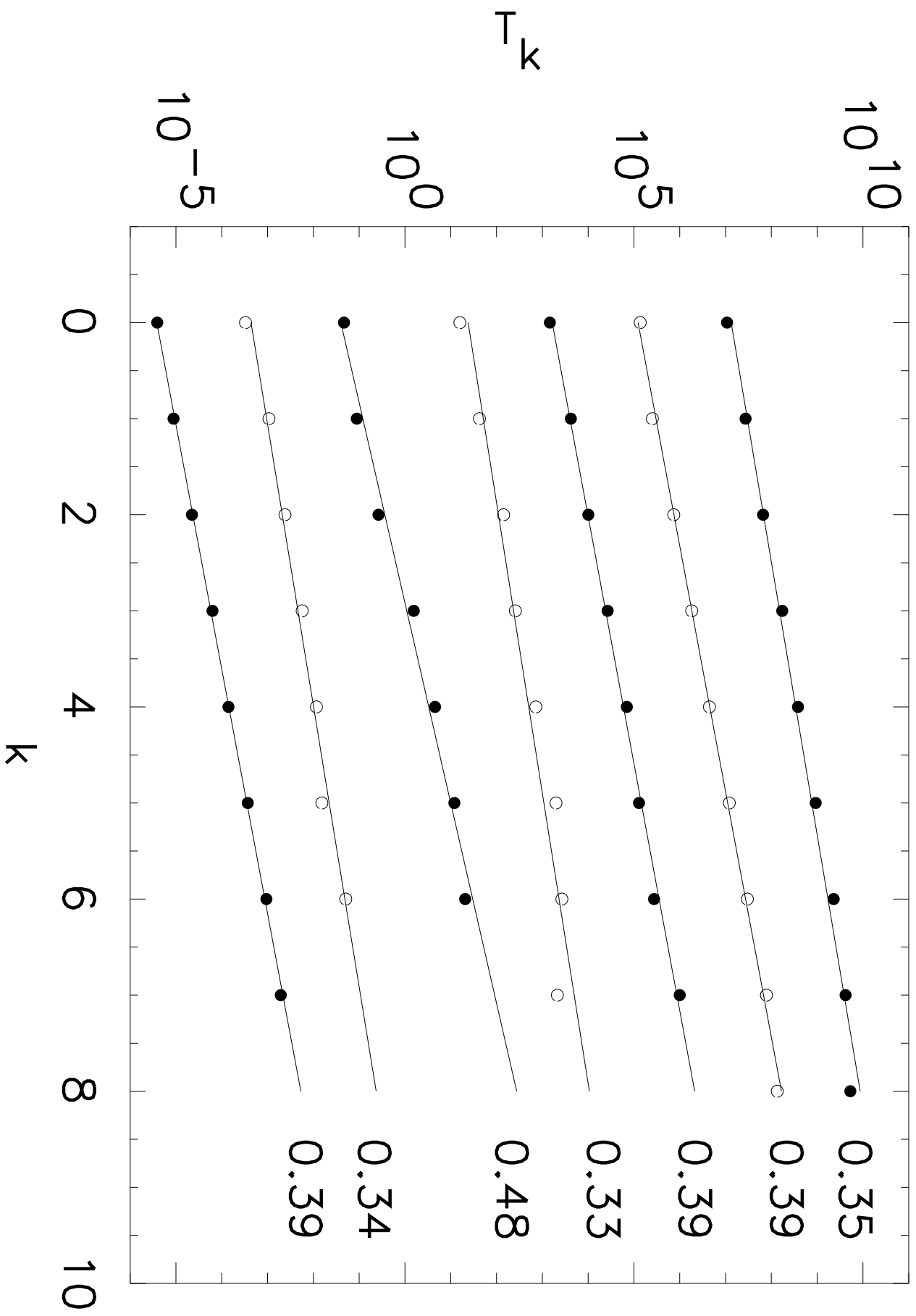




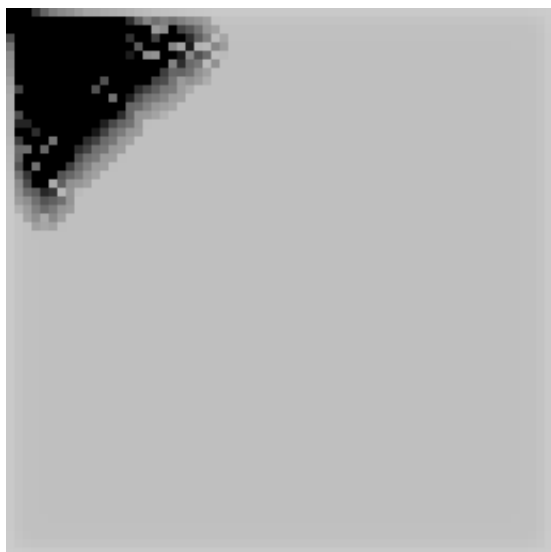




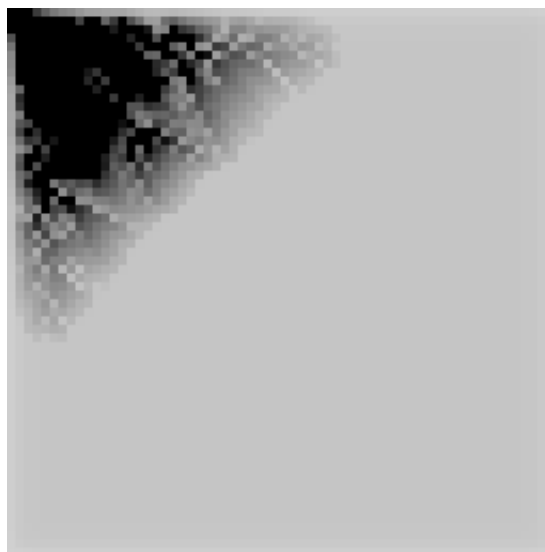




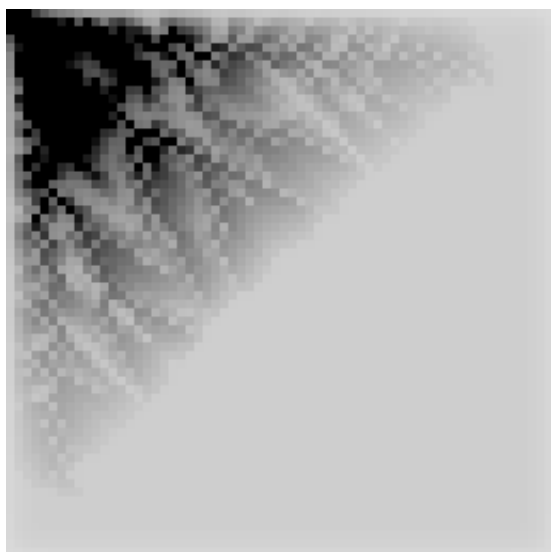
a



b



c



d

